The Astronomical Journal, 136:2391–2412, 2008 December doi:10.1088/0004-6256/136/6/2391


# A CATALOG OF EXTENDED GREEN OBJECTS IN THE GLIMPSE SURVEY: A NEW SAMPLE OF MASSIVE YOUNG STELLAR OBJECT OUTFLOW CANDIDATES

C. J. Cyganowski[1], B. A. Whitney[2], E. Holden[1], E. Braden[1], C. L. Brogan[3], E. Churchwell[1], R. Indebetouw[3,4], D. F. Watson[5], B. L. Babler[1], R. Benjamin[6], M. Gomez[7], M. R. Meade[1], M. S. Povich[1], T. P. Robitaille[8], and C. Watson[9]
[1] University of Wisconsin, Madison, WI 53706, USA; ccyganow@astro.wisc.edu
[2] Space Science Institute, 4750 Walnut St. Suite 205, Boulder, CO 80301, USA; bwhitney@spacescience.org
[3] NRAO, 520 Edgemont Rd, Charlottesville, VA 22903, USA
[4] University of Virginia, Astronomy Department, P.O. Box 3818, Charlottesville, VA 22903-0818, USA
[5] Department of Physics and Astronomy, Vanderbilt University, Nashville, TN 37235, USA
[6] Department of Physics, University of Wisconsin at Whitewater, 800 West Main Street, Whitewater, WI 53190, USA
[7] Observatorio Astronomico, Universidad Nacional de Cordoba, Argentina, Laprida 854, 5000 Cordoba, Argentina
[8] Scottish Universities Physics Alliance, School of Physics and Astronomy, University of St. Andrews, North Haugh, St. Andrews, UK
[9] Department of Physics, Manchester College, North Manchester, IN 46962, USA
*Received 2008 May 2; accepted 2008 July 18; published 2008 November 13*

## ABSTRACT

Using images from the *Spitzer* Galactic Legacy Infrared Mid-Plane Survey Extraordinaire (GLIMPSE), we have identified more than 300 extended 4.5 $\mu$m sources (Extended Green Objects (EGOs), for the common coding of the [4.5] band as green in three-color composite InfraRed Array Camera images). We present a catalog of these EGOs, including integrated flux density measurements at 3.6, 4.5, 5.8, 8.0, and 24 $\mu$m from GLIMPSE and the Multiband Imaging Photometer for *Spitzer* Galactic Plane Survey. The average angular separation between a source in our sample and the nearest *IRAS* point source is greater than 1′. The majority of EGOs are associated with infrared dark clouds (IRDCs), and where high-resolution 6.7 GHz $CH_3OH$ maser surveys overlap the GLIMPSE coverage, EGOs and 6.7 GHz $CH_3OH$ masers are strongly correlated. Extended 4.5 $\mu$m emission is thought to trace shocked molecular gas in protostellar outflows; the association of EGOs with IRDCs and 6.7 GHz $CH_3OH$ masers suggests that the extended 4.5 $\mu$m emission may pinpoint outflows specifically from massive protostars. The mid-IR colors of EGOs lie in regions of color–color space occupied by young protostars still embedded in infalling envelopes.

*Key words:* infrared: ISM – infrared: stars – ISM: jets and outflows – stars: formation

*Online-only material:* color figures, figure sets, machine readable and VO tables

## 1. INTRODUCTION

A fundamental limitation in the study of high-mass star formation is the identification of massive young stellar objects (MYSOs), particularly young MYSOs that have not yet formed hypercompact (HC) or ultracompact (UC) H II regions.[10] The largest samples assembled to date have been drawn from the *IRAS* Point Source Catalog (e.g., Sridharan et al. 2002; Molinari et al. 1996), and are limited by its poor resolution (which often blends emission from multiple sources) and positional uncertainty. The *Midcourse Space Experiment* (*MSX*) Point Source Catalog, the basis for the RMS sample (e.g., Urquhart et al. 2008; Hoare et al. 2005, 2004), represents a vast improvement, but emission from clustered sources may still be blended at the resolution of *MSX*.

Recent large-scale, high-angular-resolution *Spitzer* surveys of the Galactic plane using the InfraRed Array Camera (IRAC, 3.6, 4.5, 5.8, and 8.0 $\mu$m, resolution less than 2″ in all bands; Fazio et al. 2004) and Multiband Imaging Photometer for *Spitzer* (MIPS; resolution ∼6″ at 24 $\mu$m; Rieke et al. 2004) present an opportunity to compile a new, less-confused sample of IR-selected MYSO candidates. The IRAC 4.5 $\mu$m band provides a promising new diagnostic in the search for MYSO candidates. Extended 4.5 $\mu$m emission is a conspicuous and ubiquitous feature of *Spitzer* images of known massive star-forming regions (MSFRs), including DR21 (Davis et al. 2007; Smith et al. 2006, and references therein), S255N (Cyganowski et al. 2007), NGC6334I(N) (Hunter et al. 2006), G34.4+0.23 (Shepherd et al. 2007), and IRAS 18566+0408 (Araya et al. 2007). The IRAC 4.5 $\mu$m band contains both $H_2$ ($v$ = 0–0, S(9, 10, 11)) lines and CO ($v$ = 1–0) band heads (see Figure 1 of Reach et al. 2006). All of these lines may be excited by shocks, such as those expected when protostellar outflows crash into the ambient interstellar medium (ISM). Models of protostellar jets by Smith & Rosen (2005) predict that, of the IRAC bands, the integrated $H_2$ line luminosity will be greatest in band 2 (4.5 $\mu$m). Observationally, the extended 4.5 $\mu$m emission of the DR21 outflow has been interpreted as tracing shocked $H_2$ based on comparisons with near-IR (NIR) $H_2$ narrowband images and *ISO* spectra (Davis et al. 2007; Smith et al. 2006, and references therein).

Extended 4.5 $\mu$m emission is of particular interest as a new MYSO diagnostic because the selection effects are orthogonal to those of traditional methods of identifying MYSO candidates (e.g., applying color criteria to point source catalogs, as done for *IRAS* by Sridharan et al. 2002 and Molinari et al. 1996 and for *MSX* by Hoare et al. 2005, 2004). Even at the resolution of IRAC, the environments in which MYSOs form—clusters, infrared dark clouds (IRDCs), and nebulous regions—can complicate point-source-based selection methods. Identifying sources with extended 4.5 $\mu$m emission targets a population with ongoing outflow activity and active, rapid accretion—a short-lived, and relatively poorly understood, stage of massive protostellar evolution (see Zinnecker & Yorke 2007).

We have compiled a catalog of over 300 extended 4.5 $\mu$m sources in the Galactic Legacy Infrared Mid-Plane Survey

[10] We define MYSOs to be young stellar objects (YSOs) that will eventually become main-sequence O or early B-type stars ($M_* \gtrsim 8\ M_\odot$).

**Table 1**
Mid-IR Integrated Flux Densities: "Likely" MYSO Outflow Candidates

| Name | J2000 Coordinates | | Area ($(''')^2$) | Integrated Flux Density (mJy) | | | | Area ($(''')^2$) | Integrated Flux Density (mJy) | Saturated? | Upper Limit? |
|---|---|---|---|---|---|---|---|---|---|---|---|
| | $\alpha$ ($^h$ $^m$ $^s$) | $\delta$ ($^\circ$ $'$ $''$) | IRAC | [3.6] | [4.5] | [5.8] | [8.0] | MIPS | [24] | | |
| (1) | (2) | (3) | (4) | (5) | (6) | (7) | (8) | (9) | (10) | (11) | (12) |
| G11.92−0.61 | 18 13 58.1 | −18 54 17 | 583 | 90.7(1.7) | 334.4(3.6) | 355.8(23.7) | 197.8(36.6) | 962 | 7331.9(154.6) | Y, 24 | |
| G12.02−0.21 | 18 12 40.4 | −18 37 11 | 73 | 3.9(2.1) | 14.1(1.3) | 16.6(11.1) | 11.3(1.7) | 132 | 113.5(26.1) | N | |
| G12.91−0.03 | 18 13 48.2 | −17 45 39 | 75 | 4.9(0.1) | 42.7(0.7) | 36.8(8.4) | 24.3(5.4) | 213 | 2168.7(49.6) | N | 8, 24 |
| G14.33−0.64 | 18 18 54.4 | −16 47 46 | 163 | 12.1(0.8) | 53.8(0.7) | 123.7(8.3) | 186.3(22.8) | 346 | 4918.9(73.7) | Y, 24 | 8, 24 |
| G14.63−0.58 | 18 19 15.4 | −16 30 07 | 79 | 6.3(0.2) | 24.2(0.3) | 44.3(1.0) | 50.9(5.5) | 772 | 1563.4(105.0) | N | 24 |
| G16.61−0.24 | 18 21 52.7 | −14 35 51 | 170 | 15.0(0.3) | 43.6(2.8) | 43.7(6.4) | 21.2(13.3) | 559 | 333.3(34.7) | N | |
| G18.67+0.03 | 18 24 53.7 | −12 39 20 | 111 | 17.8(2.2) | 56.1(2.1) | 84.7(0.5) | 72.0(13.8) | 662 | 3921.3(60.5) | N | 24 |
| G18.89−0.47 | 18 27 07.9 | −12 41 36 | 85 | 6.9(2.2) | 25.4(1.8) | 24.3(21.5) | 38.6(20.9) | 138 | 475.8(74.1) | N | |
| G19.01−0.03 | 18 25 44.8 | −12 22 46 | 721 | 88.7(15.2) | 307.2(12.6) | 471.5(80.9) | 570.1(88.8) | 835 | 3468.4(287.3) | N | |
| G19.88−0.53 | 18 29 14.7 | −11 50 23 | 423 | 145.6(24.6) | 566.2(15.9) | 910.6(78.8) | 790.8(135.6) | 783 | 5055.1(14.8) | N | |
| G22.04+0.22 | 18 30 34.7 | −09 34 47 | 75 | 1.7(1.4) | 14.0(0.2) | 19.3(3.5) | 8.8(6.4) | 536 | 3293.5(193.8) | N | 24 |
| G23.01−0.41 | 18 34 40.2 | −09 00 38 | 272 | 33.1(2.3) | 225.5(3.6) | 446.7(32.9) | 221.5(30.7) | 973 | 6189.0(481.4) | Y, 24 | |
| G23.96−0.11 | 18 35 22.3 | −08 01 28 | 184 | 30.7(1.6) | 172.7(3.0) | 245.2(12.4) | 92.2(3.0) | 852 | 1636.5(99.1) | N | |
| G24.00−0.10 | 18 35 23.5 | −07 59 32 | 37 | 0.7(0.4) | 8.9(0.7) | 16.7(1.1) | 13.7(3.4) | 69 | 294.0(1.6) | N | |
| G24.17−0.02 | 18 35 25.0 | −07 48 15 | 46 | 1.9(0.6) | 8.9(0.8) | 6.9(2.8) | 5.8(5.8) | 115 | 114.4(4.1) | N | |
| G24.94+0.07 | 18 36 31.5 | −07 04 16 | 223 | 22.3(3.7) | 55.3(1.6) | 68.1(1.7) | 49.8(12.1) | 818 | 1383.1(116.5) | N | |
| G25.27−0.43 | 18 38 57.0 | −07 00 48 | 262 | 14.6(3.2) | 43.3(2.4) | 32.9(21.7) | 16.2(4.4) | 156 | 190.8(4.2) | N | |
| G27.97−0.47 | 18 44 03.6 | −04 38 02 | 202 | 8.6(1.2) | 48.0(0.3) | 83.1(12.1) | 102.6(30.8) | 484 | 1820.7(36.4) | N | 24 |
| G28.83−0.25 | 18 44 51.3 | −03 45 48 | 575 | 52.3(15.2) | 171.0(19.5) | 115.4(52.9) | 142.5(19.5) | 478 | 3635.9(64.6) | N | 8, 24 |
| G34.41+0.24 | 18 53 17.9 | +01 25 25 | 114 | 7.2(0.4) | 21.4(0.4) | 24.9(4.3) | 16.5(10.7) | 864 | 6227.1(32.4) | Y, 24 | |
| G35.03+0.35 | 18 54 00.5 | +02 01 18 | 845 | 161.6(11.8) | 501.1(7.3) | 511.9(217.8) | 279.6(438.5) | 1089 | 10181.9(231.7) | Y, 24 | 3, 4, 5, 8, 24 |
| G35.04-0.47 | 18 56 58.1 | +01 39 37 | 154 | 8.5(1.7) | 25.4(0.8) | 17.6(0.5) | 11.8(5.8) | 426 | 188.8(16.0) | N | 3, 4, 5, 8, 24 |
| G35.13−0.74 | 18 58 06.4 | +01 37 01 | 145 | 97.5(0.8) | 181.1(3.0) | 327.2(8.0) | 452.2(43.7) | 104 | 1305.5(31.1) | N | 8, 24 |
| G35.15+0.80 | 18 52 36.6 | +02 20 26 | 351 | 97.6(2.0) | 133.7(2.3) | 275.6(1.4) | 367.9(9.4) | 714 | 1880.2(33.8) | N | 3, 4, 5, 8, 24 |
| G35.20−0.74 | 18 58 12.9 | +01 40 33 | 1066 | 490.3(9.3) | 1080.3(2.7) | 1623.1(38.2) | 2879.6(97.3) | 9971 | 31704.5(530.1) | Y, 24 | |
| G35.68−0.18 | 18 57 05.0 | +02 22 00 | 117 | 5.2(0.4) | 23.3(0.8) | 8.7(0.2) | 7.9(2.5) | 449 | 485.6(40.5) | N | 8, 24 |
| G35.79−0.17 | 18 57 16.7 | +02 27 56 | 48 | 3.2(0.6) | 12.2(0.3) | 14.5(1.3) | 11.4(6.5) | 668 | 1303.1(39.0) | N | |
| G36.01−0.20 | 18 57 45.9 | +02 39 05 | 109 | 5.4(1.6) | 18.0(1.7) | 12.1(0.8) | 5.8(1.5) | 109 | 59.3(3.5) | N | |
| G37.48−0.10 | 19 00 07.0 | +03 59 53 | 107 | 7.5(1.2) | 19.0(0.8) | 40.9(4.0) | 60.7(7.1) | 714 | 1096.3(364.0) | N | |
| G39.10+0.49 | 19 00 58.1 | +05 42 44 | 120 | 11.9(0.3) | 29.2(1.0) | 23.0(0.9) | 9.7(1.8) | 876 | 1439.8(9.1) | N | |
| G40.28−0.27 | 19 05 51.5 | +06 24 39 | 114 | 17.2(0.2) | 73.4(0.4) | 127.3(3.4) | 107.7(8.1) | 2604 | 3221.2(87.5) | N | 24 |
| G44.01−0.03 | 19 11 57.2 | +09 50 05 | 117 | 30.0(0.7) | 31.7(0.6) | 29.6(1.1) | 11.8(5.8) | 63 | 16.0(3.8) | N | |
| G45.47+0.05 | 19 14 25.6 | +11 09 28 | 248 | 65.0(3.7) | 183.3(2.8) | 143.7(20.5) | 91.5(69.5) | 847 | 15702.4(806.6) | Y, 24 | |
| G49.27−0.34 | 19 23 06.7 | +14 20 13 | 441 | 82.5(11.2) | 666.3(8.0) | 1737.2(42.9) | 1880.6(144.9) | 1319 | 8677.1(174.5) | Y, 24 | |
| G54.45+1.02 | 19 28 25.7 | +19 32 20 | 50 | 4.5(0.2) | 9.4(0.0) | 15.6(1.3) | 22.7(1.8) | 52 | 93.2(2.4) | N | 24 |
| G56.13+0.22 | 19 34 51.5 | +20 37 28 | 62 | 3.6(0.1) | 9.0(0.1) | 17.0(0.4) | 22.3(0.6) | 207 | 153.5(2.4) | N | 24 |
| G58.09−0.34 | 19 41 03.9 | +22 03 39 | 79 | 10.0(0.1) | 12.2(0.3) | 7.2(0.3) | 1.1(0.8) | 582 | 57.4(1.4) | N | |
| G59.79+0.63 | 19 41 03.1 | +24 01 15 | 121 | 7.8(0.9) | 26.9(0.7) | 45.8(3.3) | 41.9(10.7) | 518 | 417.4(29.0) | N | |
| G298.26+0.74 | 12 11 47.7 | −61 46 21 | 356 | 317.1(1.6) | 605.6(0.3) | 648.8(4.5) | 536.3(8.0) | 876 | 18226.2(51.3) | Y, 24 | 24 |
| G298.89+0.37 | 12 16 37.9 | −62 13 41 | 35 | 1.9(0.1) | 3.4(0.2) | 2.7(0.4) | 0.6(0.5) | 86 | 20.2(3.0) | N | |
| G298.90+0.36 | 12 16 43.2 | −62 14 25 | 278 | 71.7(1.6) | 125.7(0.7) | 160.1(4.6) | 162.0(7.9) | 2540 | 3293.1(211.9) | N | 24 |
| G305.48−0.10 | 13 13 45.8 | −62 51 28 | 376 | 107.8(4.3) | 275.4(0.9) | 358.5(16.5) | 304.1(35.9) | 639 | 5052.2(568.7) | Y, 24 | |
| G305.52+0.76 | 13 13 29.3 | −61 59 53 | 228 | 20.7(1.0) | 48.7(0.1) | 55.8(3.1) | 22.8(3.8) | 783 | 645.6(45.5) | N | |
| G305.57−0.34 | 13 14 49.1 | −63 05 38 | 141 | 20.3(0.7) | 35.9(0.6) | 25.0(7.1) | 13.3(2.9) | 536 | 343.9(15.0) | N | |
| G305.62−0.34 | 13 15 11.5 | −63 05 30 | 85 | 15.4(0.8) | 27.1(0.3) | 27.2(3.9) | 19.0(8.7) | 478 | 1082.8(25.1) | N | |
| G305.82−0.11 | 13 16 48.6 | −62 50 35 | 84 | 15.6(0.2) | 57.5(0.4) | 64.6(1.3) | 50.0(9.2) | 484 | 1062.2(185.6) | N | 24 |
| G305.89+0.02 | 13 17 15.5 | −62 42 24 | 124 | 36.7(0.9) | 120.4(0.2) | 166.4(14.1) | 158.5(19.6) | 622 | 3639.0(77.5) | N | 24 |
| G309.15−0.35 | 13 45 51.3 | −62 33 46 | 60 | 1.8(0.1) | 7.2(0.2) | 6.6(2.9) | 8.0(4.9) | 81 | 9.3(3.3) | N | |
| G309.38−0.13(a) | 13 47 23.9 | −62 18 12 | 131 | 8.2(0.3) | 20.3(1.2) | 26.2(4.4) | 9.4(9.6) | 645 | 3852.7(54.8) | N | |
| G309.99+0.51(a) | 13 51 12.2 | −61 32 09 | 95 | 3.9(1.0) | 8.8(0.1) | 7.8(2.6) | 15.7(6.4) | 92 | 69.3(1.1) | N | |
| G310.08−0.23 | 13 53 23.0 | −62 14 13 | 128 | 53.1(1.2) | 121.6(0.8) | 183.6(1.0) | 161.7(9.9) | 605 | 2959.2(95.5) | N | |
| G312.11+0.26 | 14 08 49.3 | −61 13 25 | 98 | 10.2(0.6) | 29.0(0.4) | 17.3(8.7) | 10.2(0.7) | 708 | 2713.6(44.8) | N | |
| G317.42−0.67 | 14 51 59.2 | −60 06 06 | 102 | 22.5(1.0) | 106.3(0.5) | 222.7(3.8) | 242.0(8.7) | 668 | 1173.9(8.3) | N | 24 |
| G317.46−0.40(b) | 14 51 19.6 | −59 50 51 | 89 | 10.8(1.6) | 55.1(0.4) | 103.4(2.4) | 117.2(14.9) | 893 | 3933.1(118.5) | Y, 24 | 24 |
| G317.87−0.15 | 14 53 16.3 | −59 26 36 | 72 | 6.4(0.1) | 13.1(0.2) | 10.5(2.4) | 8.0(5.4) | 161 | 192.8(13.7) | N | |
| G317.88−0.25 | 14 53 43.5 | −59 31 35 | 73 | 11.4(0.7) | 22.1(0.1) | 19.4(4.5) | 19.0(1.1) | 46 | 17.5(1.0) | N | 24 |
| G321.94−0.01 | 15 19 43.3 | −57 18 06 | 102 | 18.9(1.1) | 98.3(0.6) | 190.8(2.6) | 173.5(5.9) | 570 | 4416.1(57.4) | N | 24 |
| G324.19+0.41 | 15 31 38.0 | −55 42 36 | 115 | 25.9(0.6) | 32.2(0.7) | 53.0(3.6) | 53.7(7.2) | 138 | 207.0(1.0) | N | 8, 24? |
| G324.72+0.34 | 15 34 57.5 | −55 27 26 | 462 | 26.4(3.6) | 86.5(2.5) | 65.6(14.9) | 12.8(7.1) | 708 | 896.7(10.8) | N | 24 |
| G326.27−0.49 | 15 47 10.8 | −55 11 12 | 547 | 147.4(11.8) | 494.5(7.1) | 921.6(14.1) | 784.5(48.6) | 737 | 3139.6(173.1) | N | 8, 24 |
| G326.31+0.90 | 15 41 35.9 | −54 03 42 | 53 | 13.5(0.5) | 27.2(0.2) | 36.0(4.3) | 45.3(3.7) | 121 | 68.2(27.5) | N | |
| G326.78−0.24 | 15 48 55.2 | −54 40 37 | 295 | 207.5(0.7) | 614.1(0.5) | 1085.6(8.5) | 1415.1(18.1) | 634 | 9509.5(101.5) | Y, 24 | |
| G326.79+0.38 | 15 46 20.9 | −54 10 45 | 406 | 171.0(2.9) | 305.0(3.2) | 348.5(25.0) | 289.1(23.0) | 697 | 3762.9(26.1) | N | |
| G326.86−0.67 | 15 51 13.6 | −54 58 03 | 226 | 13.0(0.9) | 35.8(2.1) | 62.8(4.9) | 13.6(11.2) | 109 | 130.9(11.2) | N | |
| G326.97−0.03 | 15 49 03.2 | −54 23 37 | 46 | 2.4(0.1) | 11.1(0.5) | 16.8(1.2) | 11.2(3.1) | 104 | 67.3(7.9) | N | 24 |
| G327.12+0.51 | 15 47 32.7 | −53 52 39 | 1048 | 365.3(13.0) | 964.5(4.3) | 2544.5(11.3) | 4347.8(47.4) | 962 | 19185.4(143.3) | Y, 24 | 5.8, 8 |
| G327.39+0.20 | 15 50 18.5 | −53 57 07 | 170 | 67.5(0.1) | 196.5(0.4) | 259.9(4.4) | 242.4(24.9) | 547 | 3322.0(23.5) | N | 24 |

**Table 1**
(Continued)

| Name | J2000 Coordinates | | Area ($(''')^2$) | Integrated Flux Density (mJy) | | | | Area ($(''')^2$) | Integrated Flux Density (mJy) | Saturated? | Upper Limit? |
|---|---|---|---|---|---|---|---|---|---|---|---|
| | $\alpha$ ($^h$ $^m$ $^s$) | $\delta$ ($^\circ$ $'$ $''$) | IRAC | [3.6] | [4.5] | [5.8] | [8.0] | MIPS | [24] | | |
| (1) | (2) | (3) | (4) | (5) | (6) | (7) | (8) | (9) | (10) | (11) | (12) |
| G327.40+0.44 | 15 49 19.3 | −53 45 10 | 318 | 235.6(1.7) | 876.7(5.3) | 1964.7(7.4) | 2829.9(10.5) | 841 | 11960.0(150.3) | Y, 24 | 8, 24 |
| G328.14−0.43 | 15 56 57.6 | −53 57 48 | 89 | 64.9(1.3) | 146.9(0.7) | 127.8(4.4) | 23.8(7.8) | 564 | 2567.3(15.0) | N | |
| G329.18−0.31 | 16 01 47.4 | −53 11 44 | 189 | 18.2(1.6) | 90.0(1.4) | 89.7(4.4) | 31.7(11.7) | 662 | 3969.5(28.7) | N | 24 |
| G329.47+0.52 | 15 59 36.6 | −52 22 55 | 117 | 10.3(0.8) | 28.3(1.1) | 33.7(2.6) | 6.5(3.8) | 536 | 1167.9(30.8) | N | |
| G329.61+0.11 | 16 02 03.1 | −52 35 33 | 274 | 110.8(0.9) | 498.7(0.7) | 880.5(21.7) | 1431.7(60.6) | 3312 | 8092.8(438.8) | N | 24 |
| G332.35−0.12 | 16 16 07.0 | −50 54 30 | 308 | 198.6(3.4) | 429.4(1.9) | 636.1(26.7) | 612.0(70.5) | 605 | 5557.2(162.1) | Y, 24 | 24 |
| G332.56−0.15 | 16 17 12.1 | −50 47 14 | 92 | 20.7(1.6) | 51.0(2.2) | 34.6(2.5) | 21.1(26.5) | 115 | 782.4(197.7) | N | |
| G332.81−0.70 | 16 20 48.1 | −51 00 15 | 160 | 63.2(4.6) | 182.2(5.1) | 178.6(14.6) | 180.9(81.0) | 570 | 3104.6(458.5) | N | |
| G332.94−0.69 | 16 21 18.9 | −50 54 10 | 240 | 44.7(3.8) | 215.0(2.7) | 336.7(36.1) | 354.9(43.1) | 559 | 2689.8(550.2) | N | 8 |
| G332.96−0.68 | 16 21 22.9 | −50 52 58 | 164 | 34.7(0.6) | 47.9(0.8) | 283.0(6.0) | 705.3(11.8) | 444 | 3622.0(56.8) | Y, 24 | 8 |
| G333.18−0.09 | 16 19 45.6 | −50 18 34 | 206 | 129.2(5.5) | 338.1(4.0) | 344.5(9.7) | 107.0(85.4) | 121 | 1270.5(137.7) | N | 8 |
| G335.59−0.29 | 16 30 58.5 | −48 43 51 | 982 | 132.1(11.9) | 483.8(9.9) | 466.7(54.5) | 111.3(134.4) | 2160 | 10230.0(244.0) | Y, 24 | |
| G337.30−0.87 | 16 40 31.3 | −47 51 31 | 199 | 56.5(1.3) | 111.2(0.7) | 103.8(6.8) | 38.5(22.3) | 547 | 1356.2(67.6) | N | |
| G338.39−0.40 | 16 42 41.2 | −46 43 40 | 907 | 175.8(5.4) | 336.0(12.4) | 300.4(20.1) | 117.6(63.5) | 553 | 3298.4(63.0) | N | 8, 24 |
| G339.95−0.54 | 16 49 07.9 | −45 37 59 | 170 | 41.7(1.1) | 140.3(0.8) | 188.4(12.5) | 231.6(6.9) | 766 | 7877.0(182.9) | N | |
| G340.97−1.02 | 16 54 57.3 | −45 09 04 | 304 | 12.2(5.7) | 95.5(0.1) | 75.0(30.2) | 44.4(17.8) | 680 | 591.3(89.5) | N | 8 |
| G341.24−0.27 | 16 52 37.3 | −44 28 09 | 153 | 20.8(1.2) | 57.6(0.1) | 60.6(13.9) | 38.0(18.5) | 536 | 1189.0(64.0) | N | 8, 24 |
| G341.73−0.97 | 16 57 23.1 | −44 31 35 | 334 | 73.3(2.8) | 213.2(0.8) | 295.7(6.2) | 230.9(9.1) | 530 | 1184.9(13.1) | N | |
| G341.99−0.10 | 16 54 32.8 | −43 46 45 | 276 | 48.8(2.7) | 162.0(2.3) | 192.8(7.6) | 89.1(11.7) | 691 | 2304.0(30.4) | N | |
| G343.12−0.06 | 16 58 16.6 | −42 52 04 | 894 | 196.2(2.6) | 875.6(2.7) | 1254.9(21.7) | 796.6(90.2) | 3519 | 19300.2(512.4) | Y, 24 | |
| G343.50−0.47 | 17 01 18.4 | −42 49 36 | 204 | 44.4(0.7) | 204.9(1.0) | 301.2(8.7) | 216.7(8.4) | 657 | 3482.4(41.8) | N | 24 |
| G343.72−0.18(a) | 17 00 48.3 | −42 28 25 | 197 | 33.6(6.6) | 60.2(1.3) | 55.3(3.5) | 32.6(11.7) | 495 | 905.6(21.7) | N | 24 |
| G343.72−0.18(b) | 17 00 48.1 | −42 28 37 | 59 | 4.5(0.6) | 15.4(0.1) | 18.3(4.4) | 31.4(4.9) | 472 | 1092.5(107.0) | N | 24 |
| G344.58−0.02 | 17 02 57.7 | −41 41 54 | 259 | 58.0(1.1) | 205.8(2.1) | 320.0(5.2) | 430.1(11.7) | 3663 | 12302.6(43.5) | Y, 24 | 8, 24 |
| G345.72+0.82 | 17 03 06.4 | −40 17 09 | 1231 | 149.2(6.6) | 694.6(2.6) | 1400.5(29.6) | 1371.7(80.6) | 3698 | 7499.2(73.8) | Y, 24 | 8, 24 |
| G345.99−0.02 | 17 07 27.6 | −40 34 45 | 76 | 4.7(0.2) | 20.2(1.5) | 35.4(1.6) | 11.8(1.2) | 207 | 514.3(8.1) | N | 24 |
| G347.08−0.40 | 17 12 27.2 | −39 55 18 | 72 | 51.2(0.3) | 100.7(0.0) | 101.8(2.2) | 51.8(6.0) | 173 | 2286.4(5.5) | N | 24 |
| G348.55−0.98 | 17 19 20.9 | −39 03 55 | 438 | 198.9(3.4) | 442.9(11.4) | 650.0(39.7) | 680.9(162.8) | 564 | 6324.5(109.0) | N | 8, 24 |
| G348.58−0.92 | 17 19 10.7 | −39 00 23 | 301 | 75.9(1.7) | 216.8(2.8) | 246.0(2.9) | 154.2(21.2) | 576 | 5098.8(118.3) | Y, 24 | |
| G349.15−0.98 | 17 21 04.8 | −38 34 25 | 279 | 177.9(2.6) | 355.6(2.1) | 627.0(3.1) | 918.5(6.6) | 3197 | 4861.4(159.7) | Y, 24 | 24 |

(This table is also available in machine-readable and Virtual Observatory (VO) forms in the online journal.)

Extraordinaire (GLIMPSE; Benjamin et al. 2003), called Extended Green Objects (EGOs, for the common coding of the [4.5] band as green in three-color composite IRAC images). We present this catalog, split into four subcatalogs (see Section 3). We present integrated flux densities in the IRAC 4.5 $\mu$m band for all cataloged EGOs, and investigate the nature of these sources by examining their correlations with IRDCs and 6.7 GHz Class II $CH_3OH$ masers. For those EGOs for which counterparts could be identified and photometered in all four IRAC bands and the MIPs 24 $\mu$m band, we present five-band photometry (integrated flux densities at 3.6 $\mu$m, 4.5 $\mu$m, 5.8 $\mu$m, 8.0 $\mu$m, and 24 $\mu$m), and investigate the EGOs' colors. In Section 2 we describe the data and techniques used to compile the catalog, in Section 3 we present the catalog, and in Section 4 we discuss the nature of EGOs.

## 2. THE DATA

### 2.1. Identification of EGOs

This paper catalogs EGOs identified in the GLIMPSE survey area ($10^\circ < l < 65^\circ$ and $295^\circ < l < 350^\circ$, $b = \pm 1^\circ$). To identify candidate outflows, we displayed the GLIMPSE $l \times b = 3^\circ \times 2^\circ$ ($1''.2$ per pixel) mosaics[11] as three-color images with the IRAC 3.6 $\mu$m image in blue, 4.5 $\mu$m in green, and 8.0 $\mu$m in red. Each image was searched by visual examination for extended green emission, indicating excess at 4.5 $\mu$m. The source list compiled from this search was then reviewed by two additional authors independently, and only candidates agreed upon by all three authors are included in the catalog. Images in each of the IRAC bands (3.6, 4.5, 5.8, and 8.0 $\mu$m), in the MIPS 24 $\mu$m band, and a three-color composite (3.6 $\mu$m in blue, 4.5 $\mu$m in green, and 8.0 $\mu$m in red) for all cataloged EGOs are available online; an example is shown in Figure 1.

Most cataloged EGOs are bright and relatively compact, though more extended than point sources (angular extents range from a few to more than $30''$). EGOs are readily distinguishable by eye from supernovae remnants (SNRs). The IRAC emission from SNR may be dominated by shock-excited warm molecular hydrogen (Neufeld & Yuan 2008), but SNR are generally larger, more diffuse, and more structured than EGOs (Reach et al. 2006). EGOs are also distinguishable from Planetary Nebulae (PNe), which appear red in these three-color images and generally exhibit spherical morphology at mid-IR wavelengths. There are three regimes in which our EGO catalog is likely to be incomplete: (1) extended green emission near bright sources; (2) extended green emission in sources with significant polycyclic aromatic hydrocarbon (PAH) emission; and (3) diffuse green emission extended $\lesssim 10''$. Image artifacts associated with bright IRAC sources may obscure or confuse extended 4.5 $\mu$m emission associated with these sources. Bright PAH emission (e.g., in a YSO envelope) may overwhelm extended 4.5 $\mu$m emission from an outflow. Slightly extended ($\lesssim 10''$) 4.5 $\mu$m emission may be confused with multiple nearby or blended point sources (and vice versa); requiring agreement among three observers may exclude some slightly extended sources.[12]

[11] Available at http://data.spitzer.caltech.edu/popular/glimpse/20070416_enhanced_v2/3.1x2.4_mosaics/

[12] Of 326 sources identified in the initial search, 24 (∼7%) were excluded because the three observers did not agree on their inclusion.

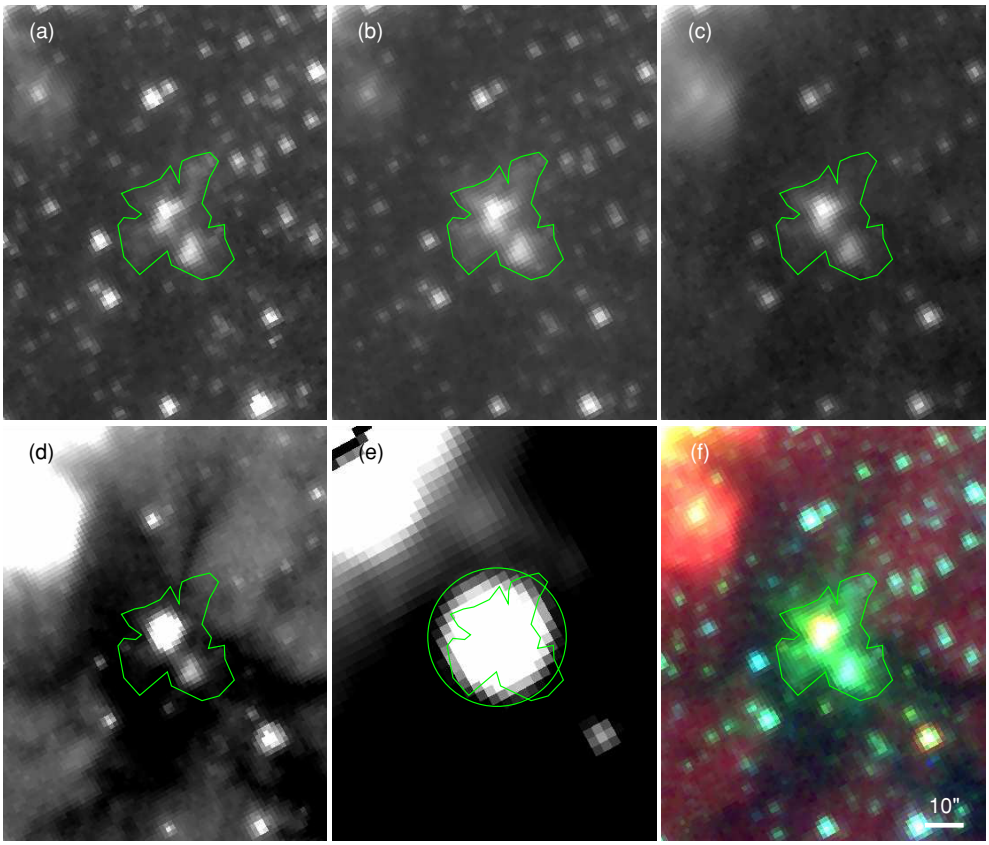


**Figure 1.** (a)–(e) IRAC (a) 3.6 $\mu$m, (b) 4.5 $\mu$m, (c) 5.8 $\mu$m, (d) 8.0 $\mu$m and (e) MIPS 24 $\mu$m images of the EGO G11.92−0.61. (f) Three-color GLIMPSE IRAC image of the EGO G11.92−0.61 showing 8.0 $\mu$m (red), 4.5 $\mu$m (green), and 3.6 $\mu$m (blue). The polygonal source aperture used for the IRAC photometry is overlaid in all panels. The circular region used for the MIPS photometry is overlaid on the 24 $\mu$m image. All panels are on the same spatial scale. This is an example of a source assigned to Table 1.

(An extended color figure set of this figure is available in the online journal.)

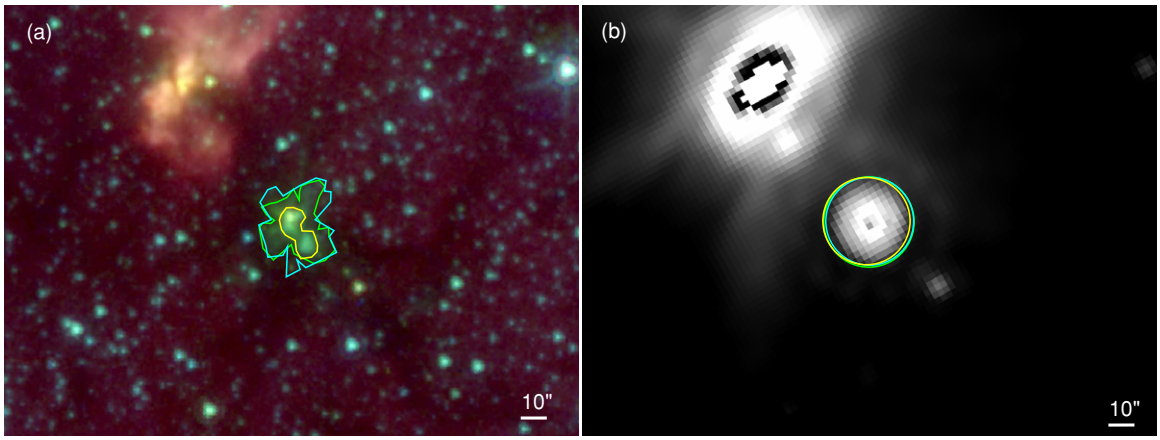


**Figure 2.** (a) Three-color GLIMPSE IRAC image of the EGO G11.92–0.61 showing 8.0 $\mu$m (red), 4.5 $\mu$m (green), and 3.6 $\mu$m (blue), with the three polygonal apertures chosen for the IRAC photometry by three different observers overlaid. (b) MIPS 24 $\mu$m image of the EGO G11.92−0.61 with the three circular apertures chosen for the MIPS photometry by three different observers overlaid. The MIPS counterpart is slightly saturated, indicated by the dip in flux at its center.

This paper does not catalog *pointlike* sources that appear green in three-color images for two reasons: (1) point sources with distinctive [3.6]–[4.5] colors may be identified via color selection in the GLIMPSE point-source catalog and archive (e.g., Ellingsen 2006, 2007); and (2) due to the flat extinction curve between 4.5 and 8.0 $\mu$m (Indebetouw et al. 2005), highly extincted stars could potentially appear green in 3.6/4.5/8.0 $\mu$m color images (e.g., Rathborne et al. 2005).

### 2.2. Photometry

Areal photometry was performed on all cataloged EGOs, using ds9 fun tools.[13] Arbitrarily shaped polygonal apertures were made to closely match the source morphology in 4.5 $\mu$m images. The same polygonal aperture was used for flux density measurements in all four IRAC bands.

[13] Available at http://hea-www.harvard.edu/saord/funtools/ds9.html

A separate aperture was made to measure the local background, the flux density was integrated over the source, and the area-corrected background was subtracted. The flux densities of EGOs at 24 $\mu$m were also measured, since this wavelength, combined with IRAC, is a good indicator of evolutionary stage in protostars (Robitaille et al. 2006). We measured 24 $\mu$m flux densities from mosaics of the Basic Calibrated Data (BCD) from the Multiband Imaging Photometer for *Spitzer* Galactic Plane Survey (MIPSGAL survey). Larger, circular or elliptical apertures were used for the 24 $\mu$m photometry because the beam size at 24 $\mu$m is at least three times larger than at IRAC wavelengths.

Most EGOs are located in areas of high and/or variable background emission, and uncertainty in the determination of the background level is a dominant contributor to the overall uncertainty in the measured flux densities. For each band, three measurements were made of the source integrated flux density, using three different background regions. Care was taken in placing the background regions to avoid bright stars and areas of exceptionally strong or weak emission. The average of the three measured source flux densities is reported in Tables 1–5, along with the standard deviation of the three measurements. The standard deviation provides an estimate of the uncertainty in the reported source flux densities resulting from uncertain background subtraction. The uncertainty due to background subtraction is generally greatest for the 8 $\mu$m flux densities, as diffuse background emission is strongest and most spatially variable in this band. The other major source of uncertainty in the measured source flux densities is observer-dependent aperture selection. To quantify this effect, a sample of 15 sources was photometered by two additional authors; Figure 2 shows the IRAC and MIPS apertures selected by the three different observers for the example source shown in Figure 1. The mean observer-dependent uncertainty is estimated to be $\sim$15% in the IRAC 3.6, 4.5, and 5.8 $\mu$m bands and the MIPS 24 $\mu$m band and about $\sim$25% in the IRAC 8.0 $\mu$m band, in addition to the background-dependent uncertainties listed in Tables 1–5.

## 3. THE CATALOGS

Tables 1–4 present the four subcatalogs of EGOs: "likely" MYSO outflow candidates are listed in Tables 1–2, "possible" MYSO outflow candidates in Tables 3–4. Table 1 presents integrated [3.6], [4.5], [5.8], [8.0], and [24] flux densities for "likely" MYSO outflow candidates with counterparts in all five bands (97 sources); for "likely" sources in which confusion and/or saturation are problematic in some bands, Table 2 presents integrated [4.5] flux densities only (36 sources). Similarly, Table 3 presents integrated [3.6], [4.5], [5.8], [8.0], and [24] flux densities for "possible" MYSO outflow candidates with counterparts in all five bands (75 sources); for "possible" sources in which confusion and/or saturation are problematic in some bands, Table 4 presents integrated [4.5] flux densities only (90 sources). Table 5 reports integrated [3.6] and [4.5] flux densities, and [3.6]–[4.5] colors, for sources in which the extended outflow emission may be photometered independently of a central source (see discussion in Section 4.3).

The sources in Tables 1–5 are organized by increasing galactic longitude. The columns in Tables 1 and 3 are Column (1), name (galactic coordinates); Columns (2) and (3), position (R.A. and decl., rounded to the nearest 0.1 s and the nearest arcsecond, respectively); Column (4), the area over which IRAC flux densities were integrated, in units of square arcseconds; Columns (5)–(8), integrated flux densities in the 3.6, 4.5, 5.8, and 8.0 $\mu$m IRAC bands (mJy), respectively; Column (9), the area over which the MIPS 24 $\mu$m flux density was integrated, in units of square arcseconds; Column (10), integrated flux density in the 24 $\mu$m MIPS band (mJy); Column (11), a flag for whether the source is saturated in any band; and Column (12), a list of bands in which the quoted flux density should be considered an upper limit because the measurement may include flux from the PSF of a nearby source. Tables 2 and 4 are similar in format, except that only [4.5] flux densities are reported.

The coordinates in Columns (2) and (3) in Tables 1–5 are those of the brightest 4.5 $\mu$m emission associated with the EGO. We emphasize that the EGOs in Tables 1–5 have angular extents on the sky ranging from a few to more than 30″, and many are near other mid-IR GLIMPSE and/or MIPS sources. To establish correlations (or the lack thereof) between the EGOs presented here and other data sets, or to plan follow-up observations, visual examination of the GLIMPSE and MIPSGAL images should be used along with the listed positions.

The errors quoted in Tables 1–5 are the standard deviations of the three measurements made with different background regions for each band (see Section 2.2). All reported flux densities are rounded to the nearest 0.1 mJy, and the reported areas are rounded to the nearest square arcsecond.

**Table 2**
[4.5] Integrated Flux Densities: "Likely" MYSO Outflow Candidates

| Name | J2000 Coordinates | | Area ((″)$^2$) | Integrated Flux Density |
|---|---|---|---|---|
| | $\alpha$ ($^h$ $^m$ $^s$) | $\delta$ ($^\circ$ ′ ″) | IRAC | (mJy) [4.5] |
| (1) | (2) | (3) | (4) | (5) |
| G10.29−0.13 | 18 08 49.3 | −20 05 57 | 69 | 13.1(1.4) |
| G10.34−0.14 | 18 09 00.0 | −20 03 35 | 94 | 72.7(4.3) |
| G16.59−0.05 | 18 21 09.1 | −14 31 48 | 128 | 50.3(0.7) |
| G19.36−0.03 | 18 26 25.8 | −12 03 57 | 153 | 115.0(2.1) |
| G19.61−0.12 | 18 27 13.6 | −11 53 20 | 102 | 32.4(5.1) |
| G25.38−0.15 | 18 38 08.1 | −06 46 53 | 46 | 46.4(0.9) |
| G28.28−0.36 | 18 44 13.2 | −04 18 04 | 112 | 47.5(3.3) |
| G34.39+0.22 | 18 53 19.0 | +01 24 08 | 307 | 20.4(4.3) |
| G48.66−0.30 | 19 21 48.0 | +13 49 21 | 120 | 2.0(0.9) |
| G49.42+0.33 | 19 20 59.1 | +14 46 53 | 98 | 12.7(0.9) |
| G309.90+0.23 | 13 51 00.4 | −61 49 53 | 109 | 16.0(0.2) |
| G317.46−0.40(a) | 14 51 19.6 | −59 50 41 | 39 | 15.3(0.4) |
| G318.04+0.09 | 14 53 39.2 | −59 09 10 | 84 | 19.6(0.2) |
| G318.05+0.09 | 14 53 42.6 | −59 08 49 | 202 | 419.5(1.3) |
| G320.23−0.28 | 15 09 52.6 | −58 25 36 | 170 | 82.4(0.8) |
| G324.17+0.44 | 15 31 24.6 | −55 41 30 | 84 | 16.4(0.1) |
| G326.32−0.39 | 15 47 04.8 | −55 04 51 | 91 | 19.1(0.0) |
| G326.47+0.70 | 15 43 15.4 | −54 07 14 | 69 | 7.8(0.2) |
| G326.48+0.70 | 15 43 17.5 | −54 07 11 | 164 | 92.5(0.3) |
| G326.61+0.80(b) | 15 43 34.6 | −53 58 00 | 84 | 17.7(0.6) |
| G328.25−0.53 | 15 57 59.7 | −53 58 00 | 523 | 866.3(3.0) |
| G329.03−0.20 | 16 00 30.6 | −53 12 34 | 397 | 81.6(1.7) |
| G329.41−0.46 | 16 03 32.4 | −53 09 26 | 219 | 258.9(3.1) |
| G329.47+0.50 | 15 59 41.0 | −52 23 28 | 219 | 59.0(1.3) |
| G330.88−0.37 | 16 10 19.9 | −52 06 13 | 88 | 41.9(1.4) |
| G331.13−0.24 | 16 10 59.8 | −51 50 19 | 46 | 21.5(0.9) |
| G332.12+0.94 | 16 10 30.4 | −50 18 05 | 121 | 43.7(0.7) |
| G332.60−0.17 | 16 17 29.4 | −50 46 13 | 82 | 14.2(2.0) |
| G332.73−0.62 | 16 20 02.8 | −51 00 32 | 186 | 80.1(3.2) |
| G333.47−0.16 | 16 21 20.2 | −50 09 50 | 117 | 125.8(0.9) |
| G335.06−0.43 | 16 29 23.1 | −49 12 28 | 157 | 46.5(1.9) |
| G335.79+0.18 | 16 29 47.1 | −48 15 47 | 134 | 93.7(1.9) |
| G337.91−0.48 | 16 41 10.3 | −47 08 06 | 613 | 1981.1(6.0) |
| G341.22−0.26(a) | 16 52 32.2 | −44 28 38 | 158 | 24.2(4.4) |
| G342.48+0.18 | 16 55 02.6 | −43 13 01 | 179 | 42.6(2.3) |
| G344.23−0.57 | 17 04 07.1 | −42 18 42 | 81 | 18.7(0.5) |

**Table 3**
Mid-IR Integrated Flux Densities: "Possible" MYSO Outflow Candidates

| Name | J2000 Coordinates | | Area ($(''')^2$) | Integrated Flux Density (mJy) | | | | Area ($(''')^2$) | Integrated Flux Density (mJy) | Saturated? | Upper Limit? |
|---|---|---|---|---|---|---|---|---|---|---|---|
| | $\alpha$ ($^h$ $^m$ $^s$) | $\delta$ ($^\circ$ $'$ $''$) | IRAC | [3.6] | [4.5] | [5.8] | [8.0] | MIPS | [24] | | |
| (1) | (2) | (3) | (4) | (5) | (6) | (7) | (8) | (9) | (10) | (11) | (12) |
| G11.11−0.11 | 18 10 28.3 | −19 22 31 | 177 | 22.2(3.7) | 200.7(1.6) | 386.7(6.1) | 263.1(24.7) | 812 | 1542.6(80.2) | N | |
| G16.58−0.08 | 18 21 15.0 | −14 33 02 | 82 | 63.7(0.5) | 63.5(0.5) | 122.6(6.5) | 83.1(23.8) | 559 | 497.9(16.6) | N | 24 |
| G24.63+0.15 | 18 35 40.1 | −07 18 35 | 52 | 8.4(0.9) | 59.8(1.7) | 103.1(1.5) | 57.9(3.5) | 530 | 405.1(125.9) | N | 24 |
| G29.84−0.47 | 18 47 28.8 | −02 58 03 | 78 | 1.4(0.8) | 14.0(0.2) | 11.2(2.2) | 7.4(3.2) | 202 | 36.4(12.4) | N | |
| G29.96−0.79 | 18 48 50.0 | −03 00 21 | 232 | 82.6(1.5) | 128.7(1.5) | 227.2(17.4) | 367.2(2.4) | 167 | 199.8(19.9) | N | 8 |
| G34.28+0.18 | 18 53 15.0 | +01 17 11 | 157 | 13.3(3.2) | 47.7(1.5) | 68.1(7.3) | 44.8(47.0) | 444 | 499.7(5.7) | N | |
| G40.28−0.22 | 19 05 41.3 | +06 26 13 | 225 | 80.6(0.8) | 236.3(0.3) | 249.1(0.5) | 204.8(1.9) | 3214 | 7733.8(198.0) | N | 24 |
| G45.80−0.36 | 19 16 31.1 | +11 16 11 | 65 | 19.1(0.2) | 63.0(0.3) | 103.8(1.4) | 108.1(3.9) | 109 | 854.1(1.2) | N | 24 |
| G49.07−0.33 | 19 22 41.9 | +14 10 12 | 48 | 23.3(0.6) | 85.9(1.0) | 135.3(0.3) | 66.1(18.9) | 98 | 381.0(57.8) | N | |
| G49.27−0.32 | 19 23 02.2 | +14 20 52 | 30 | 2.9(0.7) | 5.6(0.7) | 3.9(3.5) | 6.9(1.6) | 524 | 855.0(180.1) | N | |
| G50.36−0.42 | 19 25 32.8 | +15 15 38 | 82 | 14.4(0.5) | 20.5(0.4) | 21.3(0.6) | 11.6(2.3) | 576 | 245.4(0.3) | N | |
| G53.92−0.07 | 19 31 23.0 | +18 33 00 | 105 | 58.9(0.2) | 108.0(0.6) | 149.9(0.8) | 171.5(0.9) | 616 | 1043.1(45.1) | N | 24 |
| G54.11−0.08 | 19 31 48.8 | +18 42 57 | 58 | 54.2(0.7) | 130.4(0.7) | 244.4(5.2) | 359.0(15.5) | 559 | 2748.6(542.0) | N | |
| G54.45+1.01 | 19 28 26.4 | +19 32 15 | 91 | 23.7(0.3) | 75.8(0.4) | 147.9(1.8) | 176.6(6.2) | 588 | 1880.5(26.4) | N | 24 |
| G58.79+0.63 | 19 38 55.3 | +23 09 04 | 94 | 7.0(0.1) | 12.3(0.1) | 13.8(0.5) | 16.4(0.6) | 230 | 88.6(1.6) | N | |
| G62.70−0.51 | 19 51 51.1 | +25 57 40 | 99 | 47.8(0.2) | 64.7(0.2) | 77.1(0.3) | 74.4(1.2) | 570 | 190.0(3.8) | N | |
| G304.89+0.64 | 13 08 12.1 | −62 10 22 | 72 | 45.7(0.5) | 102.9(0.2) | 165.8(2.7) | 175.1(10.2) | 3185 | 7645.7(32.7) | Y, 24 | |
| G309.91+0.32 | 13 50 53.9 | −61 44 22 | 251 | 61.1(1.1) | 129.4(2.1) | 96.7(18.5) | 20.5(3.2) | 467 | 581.0(192.8) | N | 24 |
| G309.97+0.59 | 13 50 52.6 | −61 27 46 | 56 | 2.2(0.5) | 4.0(0.1) | 3.2(0.7) | 3.0(1.7) | 81 | 9.1(0.9) | N | |
| G309.99+0.51(b) | 13 51 12.7 | −61 32 22 | 49 | 3.1(0.4) | 7.8(0.3) | 10.7(2.0) | 2.3(1.7) | 63 | 33.2(2.7) | N | |
| G311.51−0.45 | 14 05 46.1 | −62 04 49 | 190 | 397.1(1.5) | 776.0(0.8) | 1183.6(12.8) | 1507.7(14.4) | 3070 | 10139.1(1231.5) | Y, 24 | 24 |
| G324.11+0.44 | 15 31 05.0 | −55 43 39 | 354 | 58.9(1.3) | 185.2(0.7) | 207.4(4.8) | 171.3(8.3) | 737 | 1537.6(7.1) | N | |
| G326.36+0.88 | 15 41 55.4 | −54 02 55 | 50 | 2.8(0.8) | 9.2(0.5) | 12.2(3.2) | 13.8(5.1) | 104 | 74.7(57.1) | N | |
| G326.41+0.93 | 15 41 59.4 | −53 59 03 | 343 | 75.7(3.1) | 323.6(3.1) | 468.2(24.5) | 333.4(19.0) | 772 | 2551.9(208.0) | N | 8 |
| G326.57+0.20 | 15 45 53.4 | −54 27 50 | 50 | 4.4(0.4) | 17.9(0.1) | 25.3(0.8) | 16.8(1.2) | 132 | 273.4(2.5) | N | |
| G326.61+0.80(a) | 15 43 35.1 | −53 57 36 | 150 | 20.2(0.5) | 72.9(0.8) | 115.6(4.0) | 181.7(19.0) | 484 | 2248.1(16.9) | N | 24 |
| G326.61+0.80(c) | 15 43 36.2 | −53 57 51 | 125 | 92.7(1.4) | 162.4(0.5) | 174.2(6.1) | 150.1(16.0) | 501 | 1816.6(18.0) | N | 24 |
| G326.65+0.75 | 15 44 00.9 | −53 58 45 | 140 | 40.5(0.7) | 196.8(0.4) | 300.3(4.5) | 218.2(15.8) | 507 | 2110.8(27.9) | N | 24 |
| G326.80+0.51 | 15 45 48.6 | −54 04 30 | 81 | 3.7(0.3) | 10.2(0.4) | 5.8(3.8) | 6.7(3.0) | 52 | 10.0(2.6) | N | |
| G326.92−0.31 | 15 49 56.2 | −54 38 29 | 166 | 11.0(0.9) | 60.6(0.1) | 97.8(9.6) | 84.3(30.2) | 599 | 551.4(113.4) | N | 24 |
| G327.30−0.58 | 15 53 11.2 | −54 36 48 | 89 | 24.5(1.5) | 158.8(1.7) | 341.8(8.8) | 364.9(34.1) | 369 | 2589.1(86.5) | N | 24 |
| G327.72−0.38 | 15 54 32.3 | −54 11 55 | 37 | 5.1(0.2) | 16.0(0.6) | 37.6(3.3) | 54.2(6.1) | 75 | 113.0(19.7) | N | 8, 24 |
| G327.86+0.19 | 15 52 49.2 | −53 40 07 | 52 | 7.6(0.1) | 15.9(0.4) | 26.2(1.5) | 28.8(3.6) | 305 | 339.6(45.1) | N | 8, 24 |
| G327.89+0.15 | 15 53 10.3 | −53 40 28 | 89 | 10.9(0.5) | 38.6(0.2) | 57.9(4.0) | 43.4(4.9) | 179 | 215.0(37.9) | N | |
| G328.55+0.27 | 15 56 01.5 | −53 09 44 | 157 | 85.1(2.5) | 268.8(1.2) | 368.4(10.7) | 318.4(31.4) | 812 | 4483.8(57.9) | Y, 24 | |
| G329.07−0.31(a) | 16 01 11.7 | −53 16 00 | 158 | 79.8(0.9) | 277.9(1.7) | 423.4(5.7) | 424.4(16.2) | 668 | 4192.3(39.4) | N | 24 |
| G329.07−0.31(b) | 16 01 09.9 | −53 16 02 | 217 | 57.5(0.6) | 322.8(0.4) | 795.3(5.5) | 1054.1(8.7) | 795 | 6590.2(45.9) | Y, 24 | 8, 24 |
| G329.16−0.29 | 16 01 33.6 | −53 11 15 | 36 | 4.3(0.3) | 11.8(0.0) | 16.0(1.1) | 11.8(6.3) | 75 | 106.5(1.1) | N | 24 |
| G329.18−0.30 | 16 01 44.9 | −53 11 15 | 167 | 15.5(0.8) | 66.0(1.3) | 104.6(4.1) | 50.3(19.3) | 645 | 581.7(14.6) | N | 8 |
| G331.08−0.47 | 16 11 46.9 | −52 02 31 | 111 | 6.6(1.0) | 26.6(1.7) | 60.2(5.2) | 58.7(11.9) | 415 | 629.1(79.4) | N | |
| G331.37−0.40 | 16 12 48.1 | −51 47 30 | 86 | 2.1(1.3) | 9.7(0.8) | 4.3(3.4) | 5.0(1.4) | 213 | 166.9(11.3) | N | |
| G331.62+0.53 | 16 09 56.8 | −50 56 25 | 363 | 47.6(5.6) | 117.2(2.0) | 233.2(15.1) | 444.2(25.0) | 714 | 2955.7(75.8) | N | |
| G331.71+0.58 | 16 10 06.3 | −50 50 29 | 161 | 10.7(1.0) | 26.5(0.6) | 16.6(5.0) | 10.6(6.2) | 334 | 245.5(11.7) | N | |
| G331.71+0.60 | 16 10 01.9 | −50 49 33 | 520 | 122.5(2.2) | 315.3(1.4) | 421.9(5.5) | 395.8(22.8) | 876 | 3720.8(38.6) | N | |
| G332.28−0.07 | 16 15 35.1 | −50 55 36 | 53 | 9.8(0.3) | 29.2(1.9) | 24.1(8.8) | 14.9(6.1) | 150 | 551.9(71.1) | N | 24 |
| G332.33−0.12 | 16 16 03.3 | −50 55 34 | 48 | 8.1(0.9) | 20.4(0.1) | 26.9(2.5) | 23.7(6.6) | 98 | 68.3(7.8) | N | 8 |
| G332.36+0.60 | 16 13 02.4 | −50 22 39 | 207 | 102.2(2.1) | 237.5(1.2) | 368.7(1.6) | 382.8(8.4) | 714 | 2216.9(93.4) | N | |
| G332.47−0.52 | 16 18 26.5 | −51 07 12 | 544 | 149.5(4.6) | 420.9(2.8) | 1029.5(73.0) | 1898.5(105.5) | 870 | 8610.4(182.3) | Y, 24 | |
| G332.58+0.15 | 16 16 00.6 | −50 33 30 | 69 | 7.1(0.7) | 22.0(0.9) | 24.3(4.0) | 19.2(6.4) | 167 | 203.9(17.9) | N | |
| G332.59+0.04(a) | 16 16 30.4 | −50 37 41 | 30 | 3.4(0.4) | 8.8(0.6) | 4.8(2.8) | 6.0(6.6) | 52 | 22.4(0.9) | N | |
| G332.59+0.04(b) | 16 16 30.1 | −50 37 50 | 52 | 7.9(0.6) | 20.5(0.5) | 27.2(7.2) | 41.1(6.5) | 52 | 38.1(1.9) | N | |
| G332.91−0.55 | 16 20 32.6 | −50 49 46 | 75 | 14.5(0.6) | 47.4(0.8) | 42.5(5.9) | 8.4(8.3) | 138 | 240.2(70.8) | N | |
| G333.08−0.56 | 16 21 20.9 | −50 43 05 | 151 | 37.7(3.6) | 277.3(0.7) | 558.8(37.7) | 570.9(68.6) | 513 | 1500.1(187.1) | N | |
| G334.04+0.35 | 16 21 36.9 | −49 23 28 | 177 | 31.0(1.5) | 101.9(0.4) | 171.8(1.4) | 218.7(8.7) | 645 | 2344.9(18.3) | N | |
| G334.25+0.07 | 16 23 45.2 | −49 26 32 | 86 | 8.8(0.3) | 23.4(0.6) | 24.1(2.8) | 8.7(6.4) | 138 | 201.0(11.3) | N | |
| G335.43−0.24 | 16 30 05.8 | −48 48 44 | 252 | 38.0(2.3) | 298.1(3.5) | 481.7(32.1) | 266.4(28.8) | 570 | 2380.3(39.3) | N | |
| G336.87+0.29 | 16 33 40.3 | −47 23 32 | 147 | 21.8(3.2) | 66.6(2.5) | 62.1(22.5) | 39.2(6.2) | 478 | 612.7(15.1) | N | |
| G336.96−0.98 | 16 39 37.5 | −48 10 58 | 125 | 27.1(0.2) | 64.6(0.3) | 64.1(7.2) | 42.0(2.0) | 628 | 708.6(67.2) | N | |
| G337.16−0.39 | 16 37 49.6 | −47 38 50 | 222 | 228.3(0.7) | 536.9(1.8) | 1136.5(15.3) | 2237.2(43.8) | 1140 | 5589.0(144.0) | N | 24 |
| G338.32−0.41 | 16 42 27.5 | −46 46 57 | 193 | 39.5(1.7) | 102.5(1.2) | 101.5(6.2) | 30.9(5.9) | 743 | 1479.0(46.8) | N | 8, 24 |
| G340.75−1.00 | 16 54 04.0 | −45 18 50 | 320 | 101.3(6.3) | 239.0(1.1) | 336.4(28.2) | 552.6(14.9) | 3554 | 17376.0(370.9) | Y, 24 | 24 |
| G340.77−0.12 | 16 50 17.5 | −44 43 54 | 111 | 13.1(0.6) | 34.3(0.9) | 36.3(3.9) | 28.6(13.3) | 472 | 358.6(32.1) | N | |
| G340.78−0.10 | 16 50 14.7 | −44 42 31 | 91 | 6.7(1.0) | 22.0(0.6) | 25.4(6.2) | 20.0(11.3) | 726 | 1737.9(58.7) | N | 24 |
| G341.20−0.26 | 16 52 27.8 | −44 29 29 | 58 | 23.3(0.7) | 32.3(0.1) | 33.8(3.1) | 15.5(9.1) | 144 | 49.4(9.9) | N | |
| G341.23−0.27 | 16 52 34.2 | −44 28 36 | 45 | 6.7(0.3) | 14.2(0.2) | 18.8(1.1) | 13.6(6.0) | 115 | 70.3(7.3) | N | |
| G342.15+0.51 | 16 52 28.3 | −43 16 08 | 50 | 6.6(0.2) | 12.4(0.1) | 15.7(0.4) | 16.4(0.6) | 121 | 70.5(2.5) | N | |
| G342.90−0.12 | 16 57 46.5 | −43 04 42 | 151 | 19.2(1.1) | 117.1(1.5) | 316.7(3.0) | 419.0(6.9) | 662 | 2100.0(8.1) | N | 8, 24 |
| G343.19−0.08(a) | 16 58 34.9 | −42 49 46 | 163 | 68.4(1.3) | 146.0(0.7) | 169.1(12.8) | 193.9(19.8) | 726 | 3732.1(114.7) | N | 24 |
| G343.40−0.40 | 17 00 40.4 | −42 51 33 | 66 | 17.3(0.8) | 34.5(0.8) | 47.6(2.6) | 40.2(7.5) | 109 | 94.4(10.1) | N | |

**Table 3**
(Continued)

| Name | J2000 Coordinates | | Area ($''$)$^2$) | Integrated Flux Density (mJy) | | | | Area ($''$)$^2$) | Integrated Flux Density (mJy) | Saturated? | Upper Limit? |
|---|---|---|---|---|---|---|---|---|---|---|---|
| | $\alpha$ ($^h$ $^m$ $^s$) | $\delta$ ($^\circ$ $'$ $''$) | IRAC | [3.6] | [4.5] | [5.8] | [8.0] | MIPS | [24] | | |
| (1) | (2) | (3) | (4) | (5) | (6) | (7) | (8) | (9) | (10) | (11) | (12) |
| G343.42−0.33 | 17 00 26.3 | −42 48 03 | 127 | 36.8(0.2) | 74.6(0.9) | 122.4(0.9) | 141.9(31.8) | 167 | 298.7(14.4) | N | |
| G343.50+0.03 | 16 59 10.7 | −42 31 07 | 78 | 12.7(0.4) | 27.4(0.5) | 9.5(4.9) | 31.8(1.3) | 121 | 168.6(13.9) | N | |
| G343.53−0.51(a) | 17 01 32.2 | −42 49 36 | 121 | 13.1(1.1) | 62.4(0.3) | 88.0(0.6) | 75.0(10.2) | 559 | 621.6(17.0) | N | |
| G343.78−0.24 | 17 01 13.1 | −42 27 48 | 204 | 23.3(2.1) | 50.3(2.0) | 39.7(7.9) | 15.4(7.6) | 766 | 2315.2(36.2) | N | |
| G344.21−0.62 | 17 04 17.8 | −42 21 09 | 200 | 111.5(0.2) | 272.8(1.4) | 358.0(4.3) | 320.0(11.6) | 645 | 1046.7(351.3) | N | 24 |
| G348.17+0.46 | 17 12 10.9 | −38 31 59 | 69 | 14.3(1.6) | 44.4(1.2) | 92.0(4.3) | 145.9(9.8) | 559 | 2432.5(135.0) | N | 24 |

(This table is also available in machine-readable and Virtual Observatory (VO) forms in the online journal.)

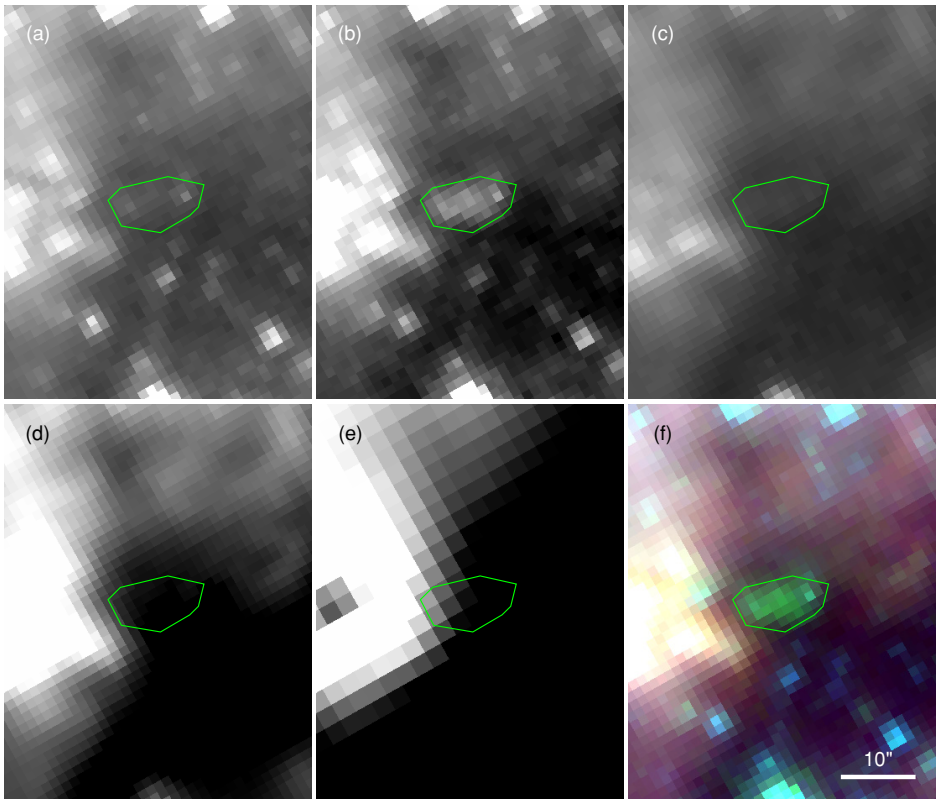


**Figure 3.** Same as Figure 1, but for the EGO G10.29−0.13. The polygonal source aperture used for the IRAC photometry is overlaid in all panels. This is an example of a source assigned to Table 2 because of the lack of clear counterparts in bands other than [4.5].

(An extended color figure set of this figure is available in the online journal.)

The categorization of an EGO as a "likely" or "possible" MYSO outflow candidate was based primarily on the angular extent of the extended excess 4.5 $\mu$m emission, e.g., the extent of diffuse green emission in three-color images. Three-color images of each EGO were reviewed by two of the authors; any source in which either observer thought it was possible that multiple nearby point sources and/or image artifacts from a bright IRAC source could be confused with truly extended 4.5 $\mu$m emission is considered a "possible" candidate. These relatively compact sources are likely still good YSO candidates (see Section 4), but not necessarily MYSOs *with outflows* and so likely to be actively accreting.

Even at the resolution of IRAC, the star-forming regions in which some EGOs are located are confused, leading to uncertainty in identifying counterparts in all five mid-IR bands (3.6, 4.5, 5.8, 8.0, and 24 $\mu$m) and in placing photometric apertures. Since the spatial resolution of MIPS at 24 $\mu$m ($\sim$6$''$) is about three times poorer than that of IRAC, sources that are distinct in IRAC images may be blended in MIPS 24 $\mu$m images. For each EGO, IRAC 3.6, 4.5, 5.8, and 8.0 $\mu$m images and the MIPS 24 $\mu$m image were displayed with the regions chosen for IRAC and MIPS photometry overlaid, as shown in Figures 1(a)–1(e). Equivalent figures for all cataloged EGOs are available online. If counterparts to the EGO are distinguishable in all bands (as in Figure 1), then five flux densities are reported (e.g., Tables 1 and 3). Examples of EGOs assigned to Tables 1–4 are shown in, respectively, Figure 1 (Table 1), Figures 3–4 (Table 2), Figure 5 (Table 3), and Figure 6 (Table 4).

## 4. DISCUSSION: THE NATURE OF EGOs

### *4.1. Infrared Associations*

The only data available for many of the EGOs in Tables 1–5 come from IR all-sky surveys, with *Spitzer* and with previous satellites. To assess whether EGOs constitute a previously unrecognized population of MYSO candidates, Table 6 lists

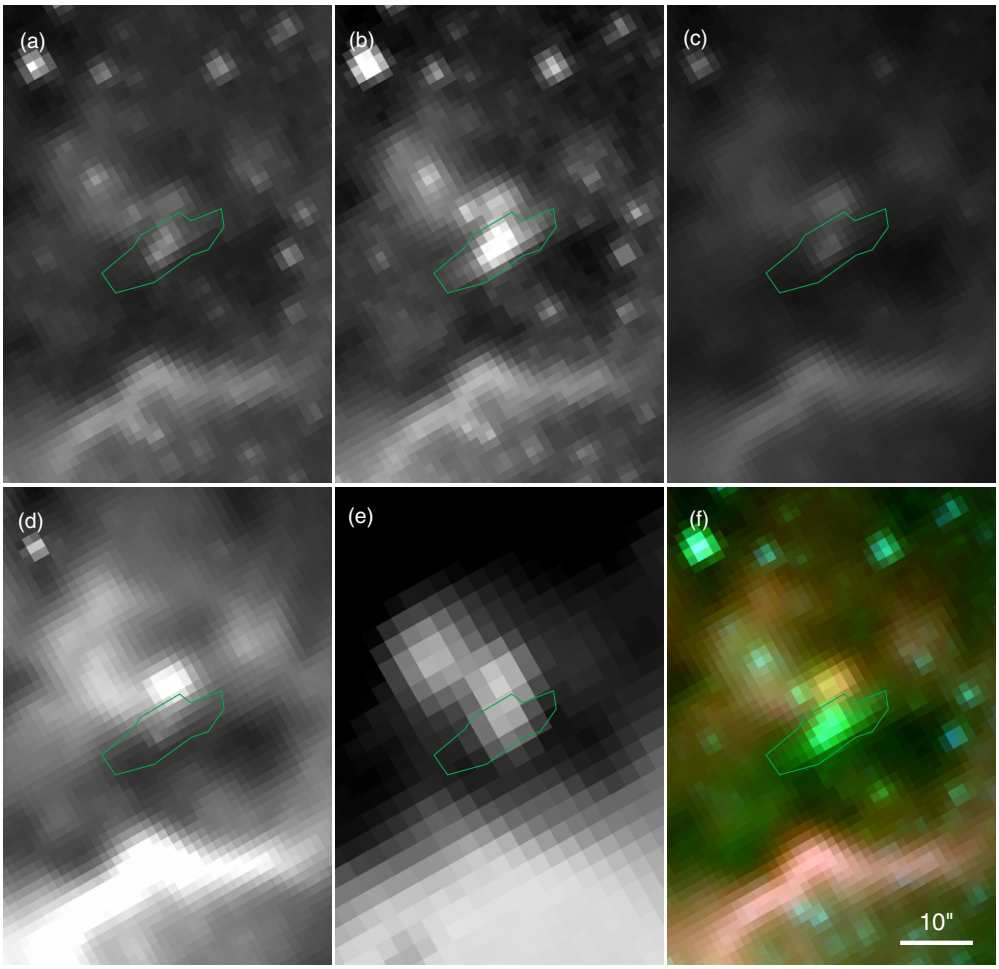


**Figure 4.** Same as Figure 1, but for the EGO G10.34−0.14, an example of a source assigned to Table 2 because of the lack of a clear counterpart at 8.0 $\mu$m and confusion in the 24 $\mu$m image. The polygonal source aperture used for IRAC photometry is overlaid in all panels.
(A color version of this figure is available in the online journal.)

the name and angular separation of the nearest *IRAS* point source (catalog version 2.1) for each cataloged EGO. Figure 7 graphically presents the data in Table 6. While some EGOs may be identified with *IRAS* point sources, and a few are well-known MYSOs (e.g., G12.91−0.26 (W33a)), the mean angular separation between a cataloged EGO and the nearest *IRAS* point source is ∼85″. The mean angular separation is ∼75″, ∼84″, ∼116″, ∼73″, and ∼40″ for EGOs in Tables 1, 2, 3, 4, and 5, respectively. Figure 8 shows the EGO G11.92–0.61 (shown in Figures 1–2) as seen by *IRAS*, *MSX*, and IRAC. As illustrated in Figure 8, the fact that most EGOs are not *IRAS* point sources does not indicate a lack of emission at the wavelengths of the *IRAS* bands, but rather in many cases is attributable to confusion and/or positional uncertainty at the resolution of *IRAS*.

IRDCs (see Simon et al. 2006a, 2006b) have been shown in recent years to be sites of the earliest stages of high-mass star formation (e.g., Rathborne et al. 2007; Rathborne et al. 2006, and references therein). IRDCs are readily visible against the diffuse background emission in GLIMPSE images, particularly at 8.0 $\mu$m. Many of these are also visible in *MSX* 8.3 $\mu$m (Band A) images and are cataloged in Simon et al. (2006a, 2006b). Small and/or filamentary IRDCs, however, may not be evident at the 20″ resolution of *MSX* Band A (∼10 times poorer than that of *Spitzer* at 8 $\mu$m). To take advantage of the higher resolution afforded by *Spitzer*, we have analyzed the correlation of EGOs with IRDCs based on visual examination of 8.0 $\mu$m GLIMPSE images.

The environment of each EGO included in Tables 1–5 was examined in 8.0 $\mu$m GLIMPSE images and IRDCs identified by visual examination; the results are tabulated in Table 6. (Note that the three-color IRAC images of each EGO available online are not, in general, scaled to highlight the presence or morphology of dark clouds.) Overall, 67% of the EGOs in Tables 1–5 are in IRDCs, many of which are small or filamentary. Of our "likely" MYSO outflow candidate EGOs, 71% are associated with IRDCs: 72% in Table 1 and 69% in Table 2. Of our "possible" MYSO outflow candidate EGOs, 64% are associated with IRDCs: 77% in Table 3 and 54% in Table 4. IRDCs are only visible in areas of high diffuse Galactic background emission, which generally decreases away from the Galactic Plane. Figure 9 shows the locations of EGOs overplotted on integrated CO emission from Dame et al. (2001), with EGOs from each of Tables 1–5 represented by a different symbol. The overall distribution pattern of EGOs with respect to CO is the same for sources from all subcatalogs: the vast majority of EGOs coincide with CO clouds. For a subset of EGOs for which we had ancillary data, we attempted to determine $v_{\rm LSR}$ from the $^{13}$CO Galactic Ring Survey (GRS; Jackson et al. 2006). Due to the presence of multiple $^{13}$CO components along the line of sight and the small angular size of EGOs however, the success rate was only ∼50%,

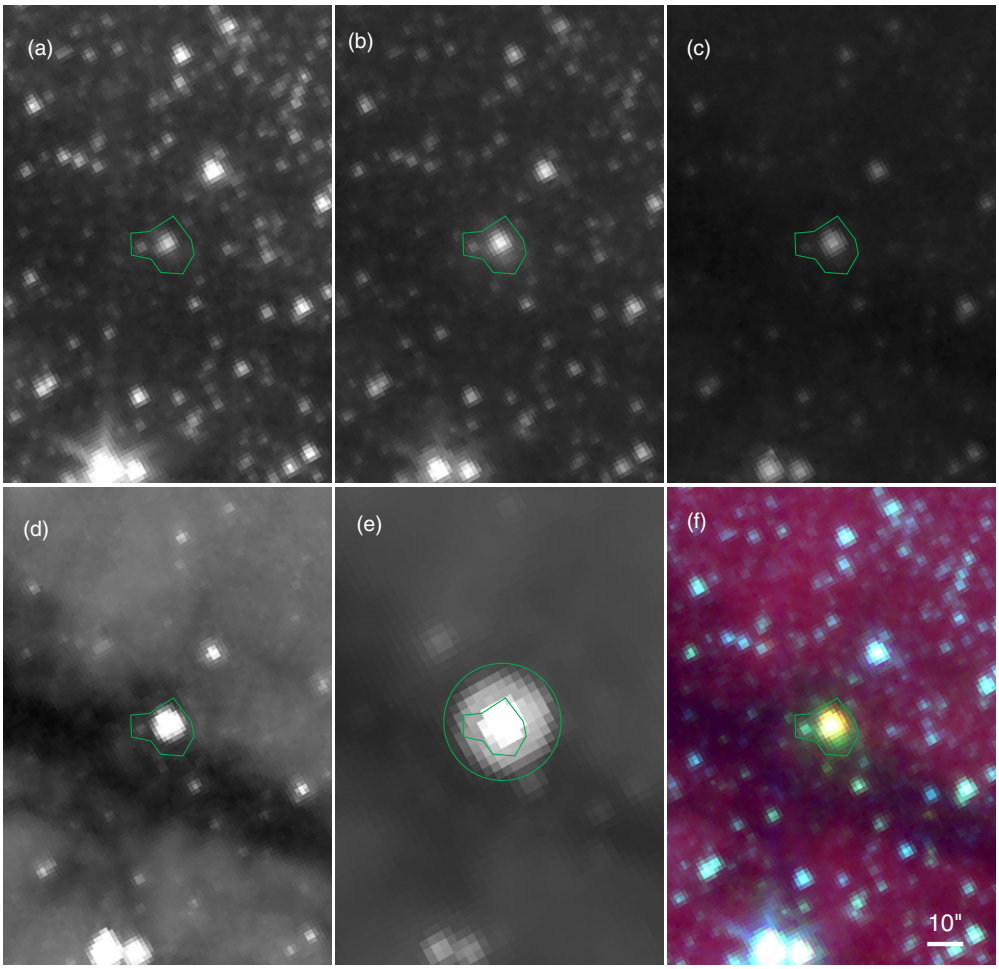


**Figure 5.** Same as Figure 1, but for the EGO G11.11−0.11, an example of a source assigned to Table 3 because, while clear counterparts are visible in all bands, the green emission is not very extended and surrounds a bright multiband IRAC source. The polygonal source aperture used for the IRAC photometry is overlaid in all panels. The circular region used for the MIPS photometry is overlaid on the 24 $\mu$m image.

(An extended color figure set of this figure is available in the online journal.)

which was not sufficiently successful to attempt for the whole sample.

The association of extended 4.5 $\mu$m emission with known MYSOs (Section 1), along with the strong correlation of EGOs with IRDCs, suggests that extended 4.5 $\mu$m emission in GLIMPSE images may be a good tracer of outflows specifically from massive YSOs. Extended 4.5 $\mu$m emission can also originate from low-mass outflows (e.g., HH46/47, Noreiga-Crespo et al. 2004; Velusamy et al. 2007). GLIMPSE is, however, a shallow survey—the faintest EGOs identified in GLIMPSE and cataloged in Tables 1–5 have surface brightnesses in 4.5 $\mu$m images of $\gtrsim$4 MJy sr$^{-1}$. In comparison, the bright knots in the HH46/47 outflow have 4.5 $\mu$m surface brightness of $\lesssim$2 MJy sr$^{-1}$, and the majority of the diffuse green emission in NGC1333 (Gutermuth et al. 2008) has 4.5 $\mu$m surface brightness of $\lesssim$4 MJy sr$^{-1}$, with very few bright areas of $\lesssim$10 MJy sr$^{-1}$. In both regions, the morphology of the diffuse 4.5 $\mu$m emission is mirrored in the other IRAC bands (e.g., Figure 1 of Velusamy et al. 2007), in contrast to most of the EGOs in our sample (see Section 4.3). Relatively faint diffuse 4.5 $\mu$m emission such as that seen in low-mass star-forming regions is unlikely to have been identified in our search of the GLIMPSE images.

### *4.2. Association with 6.7 GHz $CH_3OH$ Masers*

Further evidence that GLIMPSE-identified EGOs are massive comes from the association of EGOs with 6.7 GHz Class II $CH_3OH$ masers. Class II 6.7 GHz $CH_3OH$ masers are indicative of massive star formation (Szymczak et al. 2005; Ellingsen 2006), as they are *not* observed toward low-mass YSOs (Minier et al. 2003). These masers are radiatively pumped by IR photons emitted by warm dust in massive star-forming regions (e.g., Cragg et al. 2005, and references therein), and are thought to trace both the inner parts of outflows and disks (see De Buizer 2003). We have compared our EGO catalog with 6.7 GHz Class II $CH_3OH$ maser catalogs of Ellingsen (2006), Walsh et al. (1998), and Caswell (1996). To meaningfully assess the correlation of EGOs and 6.7 GHz $CH_3OH$ masers requires (a) maser positions known to $\sim$1″ or better, and (b) surveys covering well-defined areas on the sky. To our knowledge, the three surveys cited (and included in the analysis of GLIMPSE point sources associated with 6.7 GHz $CH_3OH$ masers conducted by Ellingsen 2006) are the only studies meeting these criteria that overlap the GLIMPSE coverage (see also Yusef-Zadeh et al. 2007 for the Galactic Center region). Of these studies, those of Ellingsen (2006) and Caswell (1996) cover

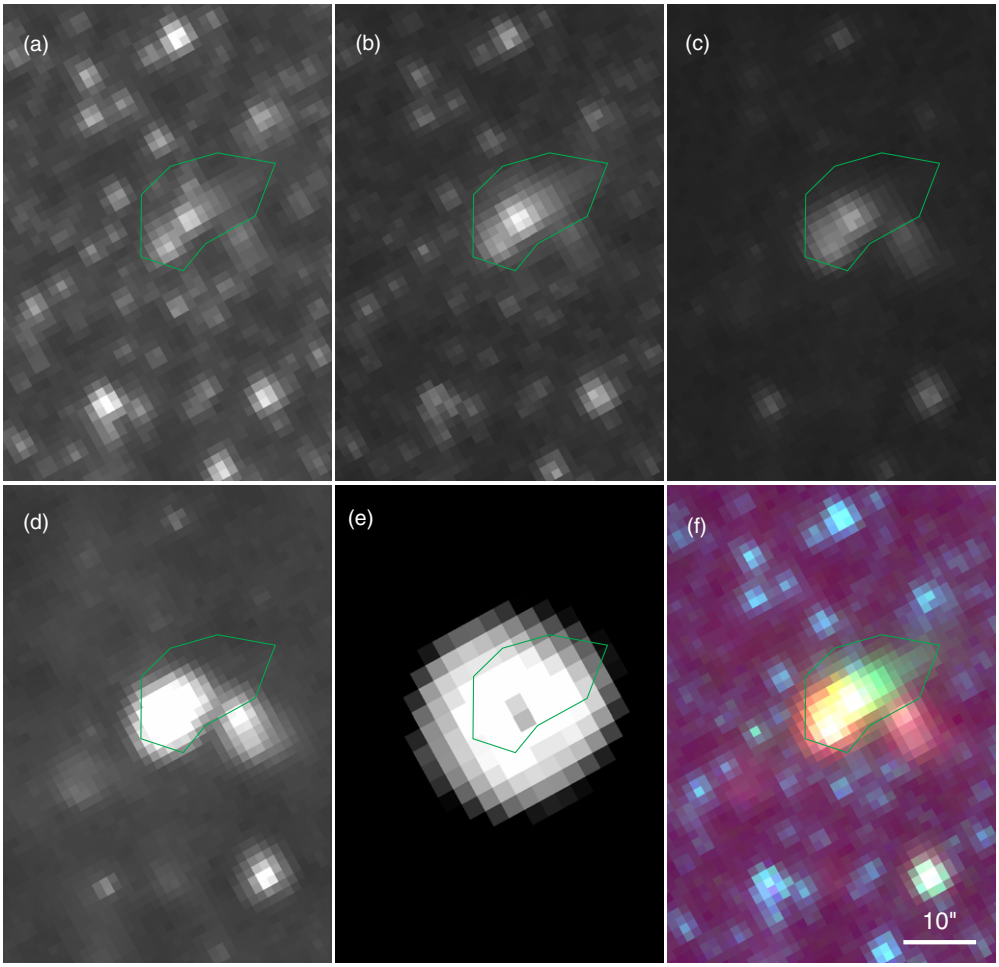


**Figure 6.** Same as Figure 1, but for the EGO G12.20−0.03, an example of a source assigned to Table 4 because of the limited extent of the 4.5 $\mu$m emission and the degree of confusion in the region. At least two multiband IRAC sources are apparent, either or both of which could be associated with the extended 4.5 $\mu$m emission; 24 $\mu$m emission from several IRAC sources appears to be blended in a single, saturated, MIPS counterpart. The polygonal source aperture used for the IRAC photometry is overlaid in all panels.

(An extended color figure set of this figure is available in the online journal.)

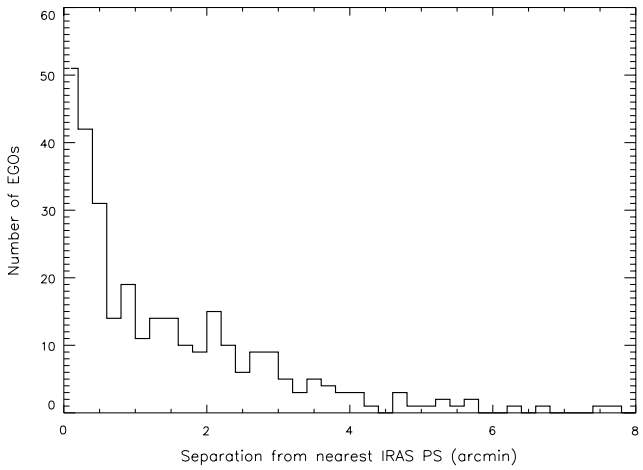


**Figure 7.** Histogram, binned to 0.′2, of number of EGOs as a function of angular separation from the nearest *IRAS* point source. About 50% of the cataloged EGO population is greater than 1′ from the nearest *IRAS* point source.

(overlapping) ranges in galactic longitude. That of Walsh et al. (1998) targeted *IRAS* sources; some EGOs serendipitously fall within the (large) primary beam. Table 7 tabulates every EGO that falls within the nominal coverage of one of these three surveys (25 EGOs from Table 1, 23 from Table 2, 26 from Table 3, 35 from Table 4, and 2 from Table 5). Column (1) lists the EGO name (galactic coordinates); Column (2), the maser survey(s) that cover the EGO position; Column (3), the *IRAS* point source targeted by Walsh et al. (1998), if relevant; Column (4), whether a maser was detected; Column (5), the nominal offset of the maser position from the EGO position (from Tables 1–5); and Column (6), the distance. The association of 6.7 GHz $CH_3OH$ maser(s) with an EGO was evaluated by plotting maser positions on images in each IRAC and the MIPS 24 $\mu$m band and on three-color IRAC images of EGOs, as illustrated in Figures 10(a)–10(f). Only masers spatially coincident with either (a) extended 4.5 $\mu$m emission, or (b) a MIPS 24 $\mu$m source or an IRAC multiband source likely to be associated with extended 4.5 $\mu$m emission, are tabulated in Table 7. Figure 11 graphically presents the nominal offsets between EGO positions (as listed in Tables 1–5) and the maser positions from the literature. As shown in Figure 11, for the vast majority of EGOs, this offset is small ($\lesssim 5''$). We emphasize that EGOs are extended on the sky, and a maser with a nominal positional offset of a few arcseconds generally lies within the area of extended 4.5 $\mu$m emission. Figures equivalent to Figure 10(a)–10(f) are available online, for all the sources listed in Table 7, to illustrate

**Table 4**
[4.5] Integrated Flux Densities: "Possible" MYSO Outflow Candidates

| Name | J2000 Coordinates | | Area ($''^2$) | Integrated Flux Density (mJy) |
|---|---|---|---|---|
| | $\alpha$ ($^h$ $^m$ $^s$) | $\delta$ ($^\circ$ $'$ $''$) | IRAC | [4.5] |
| (1) | (2) | (3) | (4) | (5) |
| G12.20−0.03 | 18 12 23.6 | −18 22 54 | 192 | 228.9(0.2) |
| G12.42+0.50 | 18 10 51.1 | −17 55 50 | 1767 | 1404.7(4.3) |
| G12.68−0.18 | 18 13 54.7 | −18 01 47 | 300 | 159.8(4.6) |
| G17.96+0.08 | 18 23 21.0 | −13 15 11 | 117 | 141.9(5.0) |
| G19.61−0.14 | 18 27 16.8 | −11 53 51 | 53 | 21.7(1.3) |
| G20.24+0.07 | 18 27 44.6 | −11 14 54 | 105 | 81.3(1.6) |
| G21.24+0.19 | 18 29 10.2 | −10 18 11 | 20 | 6.3(0.3) |
| G23.82+0.38 | 18 33 19.5 | −07 55 37 | 85 | 49.5(1.9) |
| G24.11−0.17 | 18 35 52.6 | −07 55 17 | 147 | 592.6(1.0) |
| G24.11−0.18 | 18 35 53.0 | −07 55 23 | 55 | 50.7(0.2) |
| G24.33+0.14 | 18 35 08.1 | −07 35 04 | 104 | 67.8(2.7) |
| G28.85−0.23 | 18 44 47.5 | −03 44 15 | 53 | 6.6(0.1) |
| G29.89−0.77 | 18 48 37.7 | −03 03 44 | 45 | 7.9(0.4) |
| G29.91−0.81 | 18 48 47.6 | −03 03 31 | 65 | 20.3(0.2) |
| G35.83−0.20 | 18 57 26.9 | +02 29 00 | 42 | 3.1(0.5) |
| G39.39−0.14 | 19 03 45.3 | +05 40 43 | 124 | 213.0(0.2) |
| G40.60−0.72 | 19 08 03.3 | +06 29 15 | 120 | 73.7(1.6) |
| G43.04−0.45(a) | 19 11 38.9 | +08 46 39 | 52 | 19.5(0.2) |
| G43.04−0.45(b) | 19 11 39.1 | +08 46 32 | 27 | 9.6(0.1) |
| G45.47+0.13 | 19 14 07.3 | +11 12 16 | 59 | 121.2(0.5) |
| G45.50+0.12 | 19 14 13.0 | +11 13 30 | 30 | 6.3(0.1) |
| G49.91+0.37 | 19 21 47.5 | +15 14 26 | 32 | 9.4(0.2) |
| G54.11−0.04 | 19 31 40.0 | +18 43 53 | 29 | 11.7(0.1) |
| G54.11−0.05 | 19 31 42.2 | +18 43 45 | 39 | 5.8(0.4) |
| G57.61+0.02 | 19 38 40.8 | +21 49 35 | 42 | 9.0(0.5) |
| G58.78+0.64 | 19 38 49.6 | +23 08 40 | 48 | 19.2(0.1) |
| G58.78+0.65 | 19 38 49.2 | +23 08 50 | 33 | 6.2(0.2) |
| G305.77−0.25 | 13 16 30.0 | −62 59 09 | 168 | 15.2(0.6) |
| G305.80−0.24 | 13 16 43.4 | −62 58 29 | 22 | 5.8(0.1) |
| G309.38−0.13(b) | 13 47 20.5 | −62 18 11 | 27 | 7.5(0.5) |
| G309.97+0.50 | 13 51 05.2 | −61 33 20 | 43 | 3.8(0.2) |
| G309.99+0.51(c) | 13 51 12.9 | −61 32 29 | 14 | 3.8(0.1) |
| G310.15+0.76 | 13 51 59.2 | −61 15 37 | 516 | 324.4(0.9) |
| G310.38−0.30(a) | 13 56 01.8 | −62 14 15 | 40 | 4.0(0.1) |
| G310.38−0.30(b) | 13 56 01.0 | −62 14 19 | 46 | 3.0(0.5) |
| G310.38−0.30(c) | 13 55 59.9 | −62 14 27 | 52 | 1.5(0.1) |
| G310.38−0.30(d) | 13 56 00.0 | −62 14 18 | 29 | 1.3(0.2) |
| G311.04+0.69 | 13 59 18.1 | −61 06 33 | 30 | 1.3(0.3) |
| G313.71−0.19(a) | 14 22 37.4 | −61 08 17 | 94 | 29.1(1.2) |
| G313.71−0.19(b) | 14 22 35.6 | −61 08 41 | 60 | 7.7(0.4) |
| G313.76−0.86 | 14 25 01.3 | −61 44 57 | 210 | 156.7(0.9) |
| G317.44−0.37 | 14 51 03.0 | −59 49 58 | 63 | 3.0(0.7) |
| G320.24−0.29 | 15 09 55.0 | −58 25 31 | 29 | 8.4(0.7) |
| G323.74−0.26 | 15 31 45.5 | −56 30 50 | 148 | 778.1(1.0) |
| G325.52+0.42 | 15 39 10.6 | −54 55 40 | 23 | 7.0(0.1) |
| G326.37+0.94 | 15 41 44.1 | −54 00 00 | 76 | 3.5(0.3) |
| G326.64+0.76 | 15 43 56.6 | −53 58 32 | 39 | 3.3(0.2) |
| G326.99−0.03 | 15 49 07.8 | −54 23 02 | 40 | 4.4(0.5) |
| G327.57−0.85 | 15 55 47.3 | −54 39 09 | 125 | 373.9(2.7) |
| G327.65+0.13 | 15 52 00.5 | −53 50 41 | 50 | 96.0(0.3) |
| G328.16+0.59 | 15 52 42.5 | −53 09 51 | 251 | 53.0(0.7) |
| G328.60+0.27 | 15 56 15.8 | −53 07 50 | 50 | 3.5(0.7) |
| G328.81+0.63 | 15 55 48.4 | −52 43 06 | 851 | 1461.9(5.3) |
| G330.95−0.18 | 16 09 52.7 | −51 54 56 | 181 | 225.1(0.7) |
| G331.12−0.46 | 16 11 55.3 | −52 00 10 | 58 | 6.4(0.3) |
| G331.34−0.35 | 16 12 26.4 | −51 46 17 | 94 | 460.4(1.6) |
| G331.51−0.34 | 16 13 11.7 | −51 39 12 | 102 | 4.4(0.7) |
| G332.28−0.55 | 16 17 41.8 | −51 16 04 | 53 | 8.2(0.2) |
| G332.29−0.09 | 16 15 45.2 | −50 55 52 | 62 | 153.3(0.4) |
| G332.29−0.55 | 16 17 44.3 | −51 15 42 | 26 | 3.2(0.7) |
| G332.35−0.44 | 16 17 31.4 | −51 08 22 | 33 | 11.9(0.2) |
| G333.13−0.56 | 16 21 36.1 | −50 40 49 | 386 | 38.7(4.2) |
| G333.32+0.10 | 16 19 28.9 | −50 04 40 | 60 | 19.8(0.8) |
| G335.59−0.30 | 16 31 02.5 | −48 44 07 | 176 | 21.8(0.6) |
| G336.02−0.83 | 16 35 09.7 | −48 46 44 | 226 | 49.9(1.5) |
| G336.03−0.82 | 16 35 09.6 | −48 45 55 | 35 | 10.8(0.3) |
| G337.40−0.40 | 16 38 50.4 | −47 28 04 | 386 | 354.0(4.0) |
| G338.42−0.41 | 16 42 50.5 | −46 42 29 | 256 | 30.1(2.5) |
| G338.92+0.55(a) | 16 40 33.6 | −45 41 44 | 104 | 125.8(0.6) |
| G338.92+0.55(b) | 16 40 34.1 | −45 42 07 | 230 | 750.6(2.3) |
| G339.58−0.13 | 16 45 59.5 | −45 38 44 | 222 | 232.7(1.4) |
| G340.05−0.25 | 16 48 14.7 | −45 21 52 | 128 | 27.6(2.7) |

**Table 4**
(Continued)

| Name | J2000 Coordinates | | Area ($''^2$) | Integrated Flux Density (mJy) |
|---|---|---|---|---|
| | $\alpha$ ($^h$ $^m$ $^s$) | $\delta$ ($^\circ$ $'$ $''$) | IRAC | [4.5] |
| (1) | (2) | (3) | (4) | (5) |
| G340.06−0.23 | 16 48 09.7 | −45 20 58 | 217 | 71.8(18.2) |
| G340.07−0.24 | 16 48 15.1 | −45 20 57 | 23 | 2.6(0.1) |
| G340.10−0.18 | 16 48 07.0 | −45 17 06 | 124 | 25.2(2.6) |
| G340.76−0.12 | 16 50 14.6 | −44 44 38 | 30 | 3.7(0.4) |
| G341.22−0.26(b) | 16 52 30.3 | −44 28 40 | 109 | 24.9(2.3) |
| G342.04+0.43 | 16 52 27.8 | −43 24 17 | 52 | 5.9(0.4) |
| G343.19−0.08(b) | 16 58 35.8 | −42 49 38 | 63 | 9.7(0.3) |
| G343.42−0.37 | 17 00 37.4 | −42 49 40 | 17 | 1.9(0.1) |
| G343.53−0.51(b) | 17 01 33.5 | −42 49 50 | 52 | 13.6(0.1) |
| G344.22−0.57 | 17 04 06.4 | −42 18 58 | 174 | 29.2(0.8) |
| G345.00−0.22(a) | 17 05 11.2 | −41 29 03 | 510 | 583.1(0.9) |
| G345.00−0.22(b) | 17 05 10.9 | −41 29 13 | 164 | 88.8(0.3) |
| G345.13−0.17 | 17 05 23.1 | −41 21 11 | 78 | 34.4(0.2) |
| G346.04+0.05 | 17 07 19.9 | −40 29 49 | 46 | 15.7(0.7) |
| G346.28+0.59 | 17 05 51.3 | −39 58 43 | 268 | 324.4(1.5) |
| G348.18+0.48 | 17 12 08.0 | −38 30 52 | 275 | 113.7(10.2) |
| G348.72−1.04 | 17 20 06.1 | −38 57 15 | 36 | 33.0(5.0) |
| G348.73−1.04 | 17 20 06.5 | −38 57 08 | 35 | 67.6(14.6) |

the range of projected locations of 6.7 GHz $CH_3OH$ masers relative to extended 4.5 $\mu$m emission. Among the EGOs in Table 7 are examples of masers coincident with multiband "central" sources, with 4.5 $\mu$m emission without clear counterparts in other mid-IR bands (e.g., the EGO shown in Figures 3 and 10), and with bright MIPS 24 $\mu$m point sources slightly offset from extended 4.5 $\mu$m emission (e.g., G344.23−0.57).

The nondetections in Table 7 should be treated with caution: all of the maser surveys cited are flux limited, and the sensitivity of the Walsh et al. (1998) and Caswell (1996) surveys is not uniform, but depends on the position of a source within the interferometric primary beam. This is reflected in the citations for maser detections in Column (4) of Table 7; in several cases in which an EGO fell within the nominal coverage of multiple maser surveys, a maser was detected in one survey but not in another. The fraction of EGOs within the maser survey areas found to be associated with 6.7 GHz $CH_3OH$ masers should thus be regarded as a lower limit: 73% of "likely" MYSO outflow candidate EGOs (61% in Table 1 and 86% in Table 2) and 27% of "possible" MYSO outflow candidate EGOs (4% in Table 3 and 44% in Table 4). Both of the EGOs in Table 5 that fall within the surveys' coverage have associated 6.7 GHz $CH_3OH$ masers.

Ellingsen (2006) reports kinematic distances for detected 6.7 GHz $CH_3OH$ masers; the near kinematic distances for masers from Ellingsen (2006) associated with EGOs are listed in Column (5) of Table 7. The association of EGOs with IRDCs supports the adoption of the near kinematic distance. Where two distances are listed, two masers in the Ellingsen (2006) sample appear to be associated with the EGO. The range of distances—from 2.6 to 5.3 kpc—is typical of distances to MSFR in the Galactic Plane and to IRDCs as determined by Simon et al. (2006b) from $^{13}CO$ emission.

### *4.3. Mid-IR Colors*

As illustrated in Figure 12, the integrated flux densities reported in Tables 1 and 3 are likely to be dominated by emission from the central source of an EGO, at least at wavelengths greater than 4.5 $\mu$m. As a result, the integrated flux densities may be used, with caution, to infer the properties of the

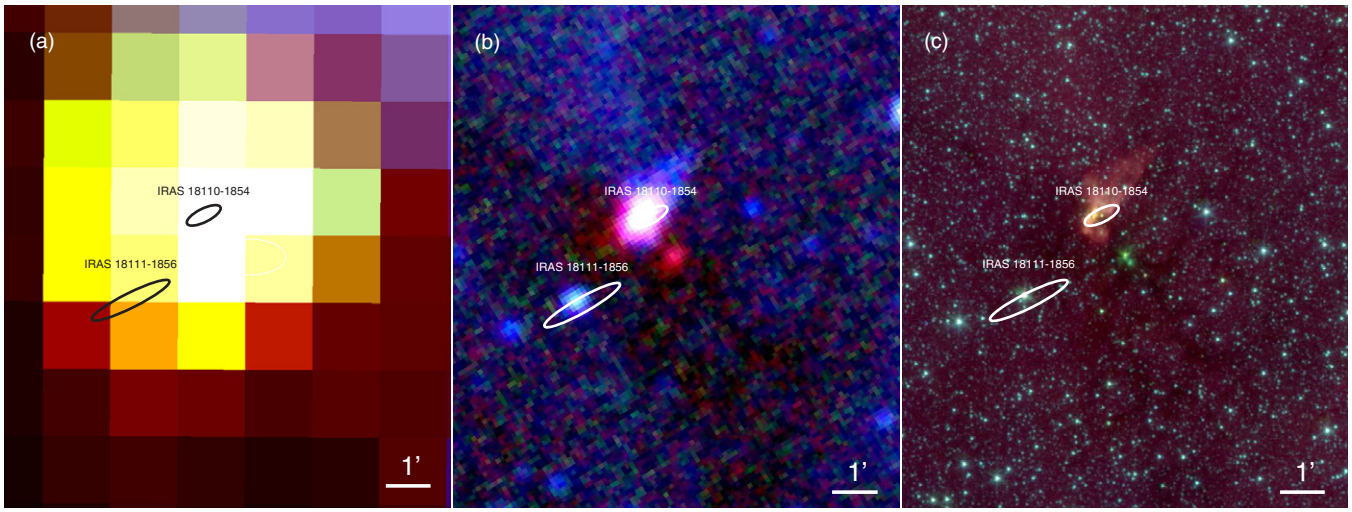


**Figure 8.** The EGO G11.92–0.61 as seen by (a) *IRAS* (red: 100 $\mu$m, green: 25 $\mu$m, blue: 12 $\mu$m), (b) *MSX* (red: 21.4 $\mu$m, green: 12.1 $\mu$m, blue: 8.3 $\mu$m, and (c) *Spitzer* IRAC (red: 8.0 $\mu$m, green: 4.5 $\mu$m, blue: 3.6 $\mu$m). Error ellipses for the two *IRAS* point sources in the field are overplotted. All panels are on the same spatial scale.

(A color version of this figure is available in the online journal.)

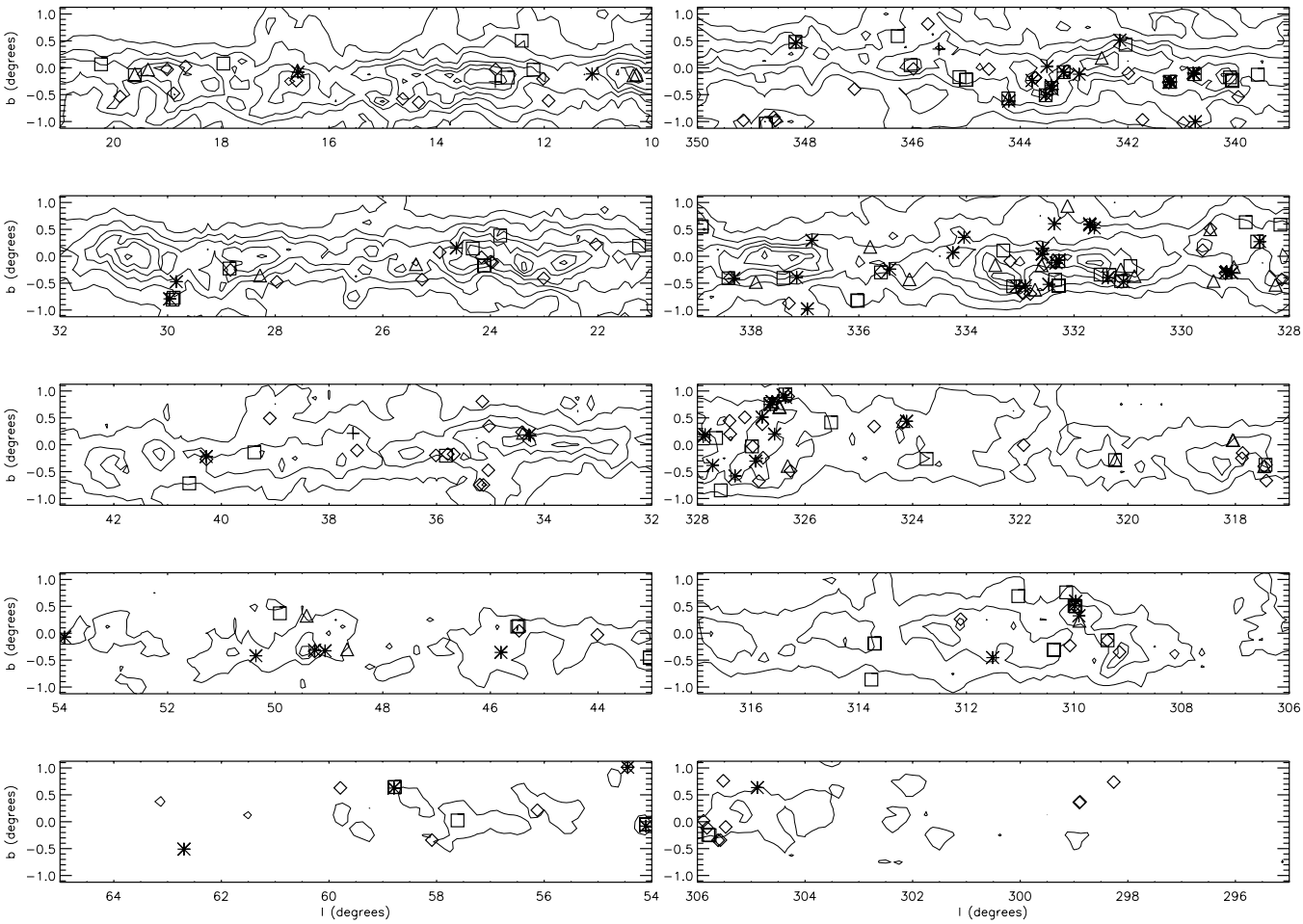


**Figure 9.** Locations of EGOs overplotted on contours of integrated CO emission from Dame et al. (2001). EGOs in Table 1 are shown as diamonds, Table 2 as squares, Table 3 as asterisks, Table 4 as triangles, and Table 5 as crosses. CO contour levels are 39.5, 79.0, 118.6, 158.1, 197.6, 237.2 K km s$^{-1}$. The overall distribution pattern of EGOs with respect to CO is the same for sources from all subcatalogs: the vast majority of EGOs coincide with CO clouds.

sources responsible for driving the hypothesized outflows traced by extended 4.5 $\mu$m emission. Figure 13 shows that EGOs are found in the region of color–color space occupied by very young YSOs, surrounded by substantial accreting envelops (Robitaille et al. 2006). Detailed spectral energy distribution (SED) fitting has not been attempted because without long-wavelength

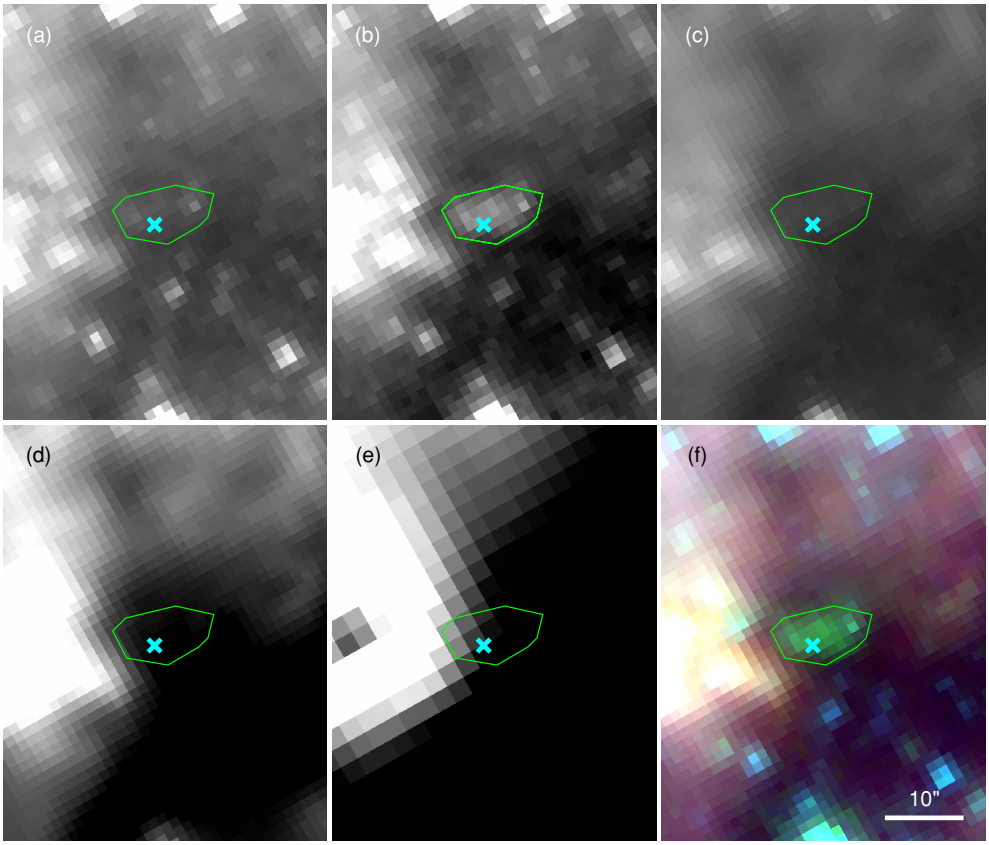


**Figure 10.** Same as Figure 3, but with a 6.7 GHz $CH_3OH$ maser from Walsh et al. (1998) marked. The region used for IRAC photometry is also overplotted. Similar images are available online for all EGOs associated with 6.7 GHz $CH_3OH$ masers in the surveys of Caswell (1996),Walsh et al. (1998) and Ellingsen (2006).
(An extended color figure set of this figure is available in the online journal.)

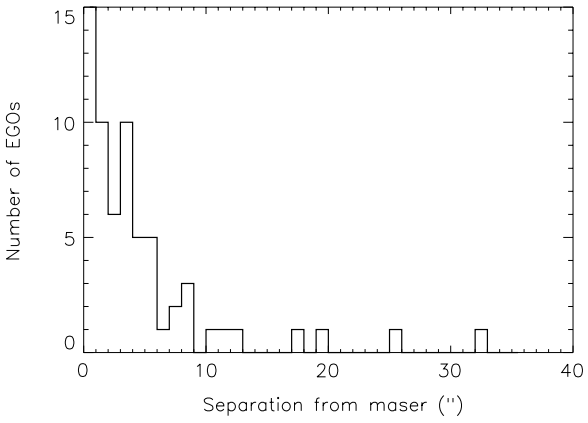


**Figure 11.** Histogram, binned to 1.″0, of number of EGOs as a function of angular separation from associated 6.7 GHz $CH_3OH$ masers. This nominal offset is small ($\lesssim 5''$ for the majority of EGOs). This is consistent with our criteria for indicating a maser association in Table 7: a maser spatially coincident either with extended 4.5 $\mu$m emission or with a 24 $\mu$m or multiband IRAC source likely to be associated with extended 4.5 $\mu$m emission.

information the SEDs are poorly constrained, and the resolution of MIPSGAL at 70 $\mu$m is too poor to resolve EGOs in crowded regions.

The EGO shown in Figure 12 is a rare example of an EGO in which a central source is sufficiently distinct that the extended "outflow" emission may be photometered separately. As shown in Figures 12(a)–12(e), the extended 4.5 $\mu$m emission evident in Figure 12(b) has a comparably extended counterpart only in the 3.6 $\mu$m band. Table 5 reports 3.6 $\mu$m and 4.5 $\mu$m integrated flux densities for the "outflow-only" regions shown in Figure 12(f) and for four additional sources in which "outflow-only" regions can be distinguished (shown in the online version of Figure 12). The [3.6]–[4.5] colors of the extended emission in these five sources fall within the range determined for "the shocked outflow nebulosity" in the DR21 outflow by Smith et al. (2006) and redward in [3.6]–[4.5] space of the nonoutflow "surrounding nebulosity" (see Figure 7 of Smith et al. 2006).

## 5. CONCLUSIONS

We have cataloged over 300 EGOs, identified by their extended 4.5 $\mu$m emission, in GLIMPSE images. The suggestion that extended 4.5 $\mu$m emission in GLIMPSE traces outflows specifically from *massive* YSOs is supported by the strong correlation of EGOs with IRDCs and 6.7 GHz Class II $CH_3OH$ masers, both associated with early stages of massive star formation. The mid-IR colors of EGOs lie in regions of color–color space occupied by young protostars still embedded in infalling envelopes. Taken together, this evidence suggests that *Spitzer* images (e.g., the GLIMPSE I, II, and 3D surveys and other Galactic programs) may be used to identify a large number of new MYSO candidates *that are actively accreting*, a crucial category of sources for constraining models of high-mass star formation.

The catalog presented here represents a source list for further study. Most of the candidates have not been previously studied,

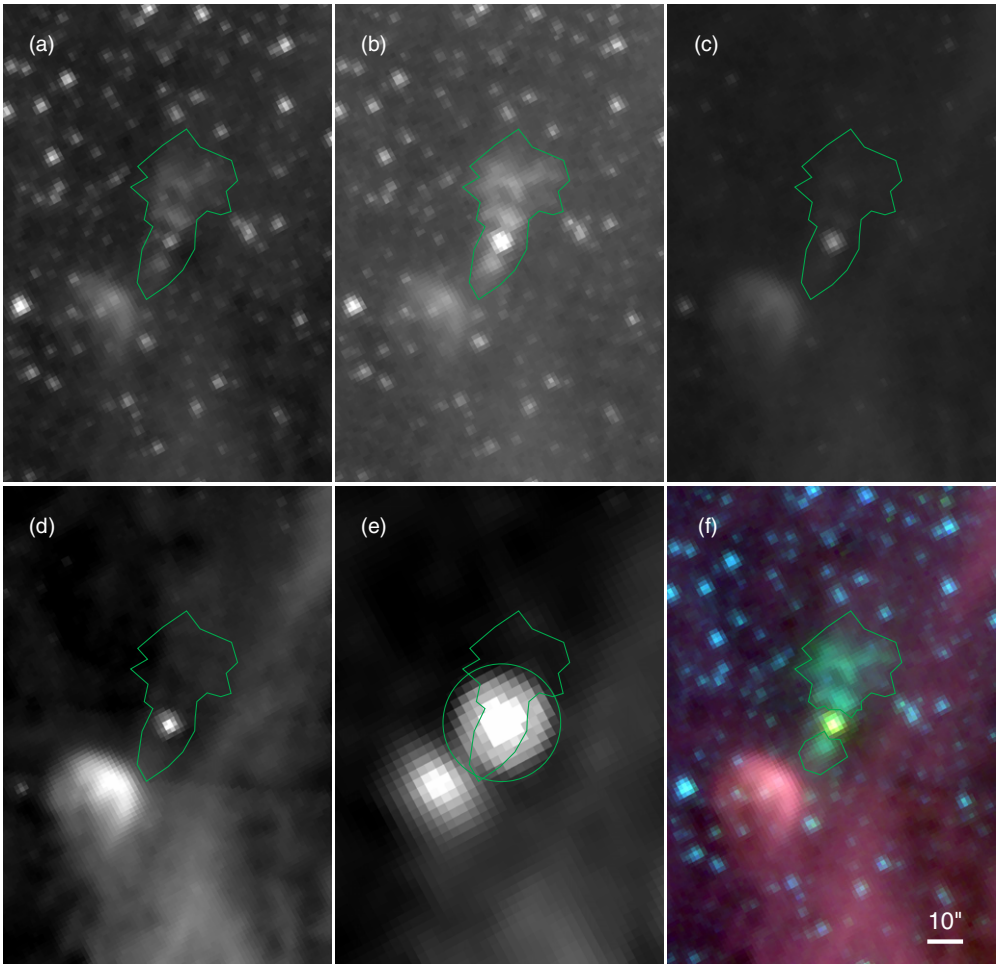


**Figure 12.** (a)–(e) IRAC (a) 3.6 $\mu$m, (b) 4.5 $\mu$m, (c) 5.8 $\mu$m, (d) 8.0 $\mu$m, and (e) MIPS 24 $\mu$m images of the EGO G19.01−0.03. The polygonal aperture used for the photometry reported in Table 1 is shown in all panels; the aperture used for MIPS 24 $\mu$m photometry is also shown in panel (e). (f) Three-color GLIMPSE IRAC image of the EGO G19.01−0.03 showing 8.0 $\mu$m(red), 4.5 $\mu$m(green), and 3.6 $\mu$m(blue) with the polygonal source apertures used for "outflow-only" IRAC photometry reported in Table 5 overlaid. All panels are on the same spatial scale. The central point source dominates the flux density in the IRAC Table 1 aperture at wavelengths longer than 4.5 $\mu$m.

(An extended color figure set of this figure is available in the online journal.)

**Table 5**
"Outflow-Only" [3.6] and [4.5] Integrated Flux Densities

| Name | J2000 Coordinates | | Area ($(''')^2$) | Integrated Flux Density (mJy) | | [3.6]–[4.5] |
|---|---|---|---|---|---|---|
| | $\alpha$ ($^h$ $^m$ $^s$) | $\delta$ ($^\circ$ $'$ $''$) | IRAC | [3.6] | [4.5] | |
| (1) | (2) | (3) | (4) | (5) | (6) | (7) |
| G12.91−0.26 | 18 14 39.5 | −17 52 00 | 965 | 172.3(13.2) | 385.7(23.4) | 0.87 |
| G19.01−0.03 O–N[a] | 18 25 44.8 | −12 22 46 | 507 | 66.2(4.3) | 141.3(3.0) | 0.82 |
| G19.01−0.03 O–S[a] | 18 25 44.8 | −12 22 46 | 98 | 11.7(0.7) | 28.5(1.3) | 0.97 |
| G34.26+0.15 | 18 53 16.4 | +01 15 07 | 3787 | 324.8(8.6) | 838.9(15.6) | 1.03 |
| G37.55+0.20 | 18 59 07.5 | +04 12 31 | 626 | 13.3(3.5) | 39.2(5.4) | 1.17 |
| G345.51+0.35 | 17 04 24.6 | −40 43 57 | 1407 | 244.4(11.4) | 386.7(9.3) | 0.50 |

**Note.** [a] Coordinates are for the central source of the EGO G19.01–0.03, as given in Table 1.

and broadband *Spitzer* images are insufficient to ensure a homogeneous pool of candidates. We have selected a sample of ∼30 northern EGOs for extensive follow-up observations designed to test the hypothesis that 4.5 $\mu$m emission traces shocked gas in outflows from MYSOs. This sample was chosen to span a range of 4.5 $\mu$m morphologies and associations (or lack thereof) with other tracers of massive star formation. We will report the results of these studies in subsequent papers.

This work is based on observations made with the *Spitzer Space Telescope*, which is operated by the Jet Propulsion Laboratory, California Institute of Technology under a contract with NASA. This work was based on data taken by the GLIMPSE and MIPSGAL *Spitzer Space Telescope* Legacy Programs. This research has made use of NASA's Astrophysics Data System Bibliographic Services and the SIMBAD database operated at CDS, Strasbourg, France. Support for this work was

**Table 6**
Infrared EGO Associations

| Name (1) | IRDC? (2) | Nearest *IRAS* PS[a] (3) | Angular Separation (″) (4) |
|---|---|---|---|
| Table 1 | | | |
| G11.92−0.61 | Y | 18110−1854 | 62 |
| G12.02−0.21 | Y | 18097−1835 | 137 |
| G12.91−0.03 | Y | 18111−1746 | 200 |
| G14.33−0.64 | Y | 18159−1648 | 15 |
| G14.63−0.58 | Y | 18164−1631 | 34 |
| G16.61−0.24 | Y | 18190−1435 | 133 |
| G18.67+0.03 | N | 18220−1241 | 36 |
| G18.89−0.47 | Y | 18242−1241 | 113 |
| G19.01−0.03 | Y | 18228−1224 | 88 |
| G19.88−0.53 | Y | 18264−1152 | 6 |
| G22.04+0.22 | Y | 18278−0936 | 5 |
| G23.01−0.41 | N | 18318−0901 | 130 |
| G23.96−0.11 | N | 18326−0802 | 113 |
| G24.00−0.10 | Y | 18326−0802 | 50 |
| G24.17−0.02 | Y | 18326−0751 | 64 |
| G24.94+0.07 | N | 18337−0707 | 78 |
| G25.27−0.43 | Y | 18362−0703 | 29 |
| G27.97−0.47 | Y | 18412−0440 | 116 |
| G28.83−0.25 | Y | 18421−0348 | 35 |
| G34.41+0.24 | Y | 18507+0121 | 31 |
| G35.03+0.35 | N | 18515+0157 | 58 |
| G35.04−0.47 | Y | 18545+0134 | 135 |
| G35.13−0.74 | N | 18553+0133 | 215 |
| G35.15+0.80 | N | 18500+0216 | 24 |
| G35.20−0.74 | N | 18556+0136 | 4 |
| G35.68−0.18 | Y | 18547+0215 | 246 |
| G35.79−0.17 | Y | 18547+0223 | 10 |
| G36.01−0.20 | Y | 18551+0238 | 194 |
| G37.48−0.10 | N | 18574+0355 | 191 |
| G39.10+0.49 | N | 18585+0538 | 5 |
| G40.28−0.27 | Y | 19034+0618 | 70 |
| G44.01−0.03 | N | 19094+0944 | 79 |
| G45.47+0.05 | Y | 19120+1103 | 59 |
| G49.27−0.34 | Y | 19207+1410 | 221 |
| G54.45+1.02 | N | 19262+1925 | 12 |
| G56.13+0.22 | N | 19326+2030 | 19 |
| G58.09−0.34 | Y | 19388+2156 | 23 |
| G59.79+0.63 | Y | 19389+2354 | 10 |
| G298.26+0.74 | N | 12091−6129 | 3 |
| G298.89+0.37 | Y | 12140−6157 | 76 |
| G298.90+0.36 | N | 12140−6157 | 19 |
| G305.48−0.10 | N | 13108−6233 | 191 |
| G305.52+0.76 | Y | 13102−6143 | 12 |
| G305.57−0.34 | Y | 13113−6249 | 109 |
| G305.62−0.34 | N | 13119−6249 | 7 |
| G305.82−0.11 | Y | 13128−6236 | 291 |
| G305.89+0.02 | Y | 13140−6226 | 27 |
| G309.15−0.35 | Y | 13421−6217 | 125 |
| G309.38−0.13(a) | Y | 13438−6203 | 32 |
| G309.99+0.51(a) | Y | 13475−6115 | 129 |
| G310.08−0.23 | Y | 13497−6159 | 31 |
| G312.11+0.26 | Y | 14050−6056 | 171 |
| G317.42−0.67 | Y | 14481−5953 | 5 |
| G317.46−0.40(b) | Y | 14480−5941 | 313 |
| G317.87−0.15 | Y | 14488−5915 | 276 |
| G317.88−0.25 | Y | 14500−5918 | 78 |
| G321.94−0.01 | Y | 15158−5707 | 34 |
| G324.19+0.41 | N | 15277−5532 | 39 |
| G324.72+0.34 | Y | 15310−5517 | 13 |
| G326.27−0.49 | Y | 15432−5501 | 7 |
| G326.31+0.90 | Y | 15375−5352 | 168 |
| G326.78−0.24 | N | 15450−5431 | 7 |

**Table 6**
(Continued)

| Name (1) | IRDC? (2) | Nearest *IRAS* PS[a] (3) | Angular Separation (″) (4) |
|---|---|---|---|
| G326.79+0.38 | Y | 15425−5401 | 2 |
| G326.86−0.67 | Y | 15475−5449 | 104 |
| G326.97−0.03 | Y | 15453−5416 | 164 |
| G327.12+0.51 | N | 15437−5343 | 4 |
| G327.39+0.20 | N | 15464−5348* | 4 |
| G327.40+0.44 | Y | 15454−5335 | 29 |
| G328.14−0.43 | Y | 15529−5350 | 94 |
| G329.18−0.31 | Y | 15579−5303 | 8 |
| G329.47+0.52 | Y | 15557−5215 | 53 |
| G329.61+0.11 | Y | 15584−5230 | 208 |
| G332.35−0.12 | Y | 16122−5047 | 18 |
| G332.56−0.15 | Y | 16132−5039 | 97 |
| G332.81−0.70 | N | 16170−5053 | 48 |
| G332.94−0.69 | Y | 16175−5046 | 22 |
| G332.96−0.68 | Y | 16175−5045 | 3 |
| G333.18−0.09 | Y | 16159−5012 | 75 |
| G335.59−0.29 | Y | 16272−4837 | 21 |
| G337.30−0.87 | Y | 16366−4746 | 82 |
| G338.39−0.40 | Y | 16390−4637 | 25 |
| G339.95−0.54 | N | 16455−4531 | 90 |
| G340.97−1.02 | Y | 16513−4504 | 48 |
| G341.24−0.27 | Y | 16487−4423 | 170 |
| G341.73−0.97 | Y | 16537−4426 | 3 |
| G341.99−0.10 | Y | 16510−4341 | 55 |
| G343.12−0.06 | Y | 16547−4247 | 4 |
| G343.50−0.47 | N | 16579−4245 | 120 |
| G343.72−0.18(a) | Y | 16572−4221 | 137 |
| G343.72−0.18(b) | Y | 16574−4225 | 133 |
| G344.58−0.02 | N | 16594−4137 | 9 |
| G345.72+0.82 | Y | 16596−4012 | 0.4 |
| G345.99−0.02 | N | 17039−4030 | 14 |
| G347.08−0.40 | Y | 17089−3951 | 9 |
| G348.55−0.98 | N | 17158−3901 | 64 |
| G348.58−0.92 | Y | 17157−3855 | 129 |
| G349.15−0.98 | Y | 17176−3831 | 0.8 |
| | 70/97 | avg./median | 75/50 |
| Table 2 | | | |
| G10.29−0.13 | Y | 18060−2005 | 134 |
| G10.34−0.14 | Y | 18060−2005 | 111 |
| G16.59−0.05 | Y | 18182−1433 | 19 |
| G19.36−0.03 | Y | 18236−1205 | 24 |
| G19.61−0.12 | N | 18244−1155 | 43 |
| G25.38−0.15 | Y | 18355−0650 | 110 |
| G28.28−0.36 | N | 18416−0420 | 81 |
| G34.39+0.22 | Y | 18507+0121 | 52 |
| G48.66−0.30 | Y | 19199+1347 | 463 |
| G49.42+0.33 | N | 19186+1440 | 34 |
| G309.90+0.23 | Y | 13475−6135 | 54 |
| G317.46−0.40(a) | Y | 14480−5941 | 319 |
| G318.04+0.09 | Y | 14498−5856 | 24 |
| G318.05+0.09 | N | 14498−5856 | 9 |
| G320.23−0.28 | Y | 15061−5814 | 82 |
| G324.17+0.44 | N | 15277−5532 | 102 |
| G326.32−0.39 | N | 15428−5453 | 213 |
| G326.47+0.70 | Y | 15394−5358 | 27 |
| G326.48+0.70 | Y | 15394−5358 | 20 |
| G326.61+0.80(b) | Y | 15395−5348 | 89 |
| G328.25−0.53 | N | 15541−5349 | 3 |
| G329.03−0.20 | Y | 15566−5304 | 2 |
| G329.41−0.46 | N | 15596−5301 | 11 |
| G329.47+0.50 | Y | 15557−5215 | 48 |
| G330.88−0.37 | Y | 16065−5158 | 20 |
| G331.13−0.24 | N | 16071−5142 | 28 |

**Table 6**
(Continued)

| Name (1) | IRDC? (2) | Nearest *IRAS* PS[a] (3) | Angular Separation (″) (4) |
|---|---|---|---|
| G332.12+0.94 | Y | 16067−5010 | 10 |
| G332.60−0.17 | Y | 16136−5038 | 69 |
| G332.73−0.62 | Y | 16158−5055 | 262 |
| G333.47−0.16 | N | 16175−5002 | 14 |
| G335.06−0.43 | Y | 16256−4905 | 17 |
| G335.79+0.18 | Y | 16259−4805 | 224 |
| G337.91−0.48 | N | 16374−4701 | 42 |
| G341.22−0.26(a) | Y | 16487−4423 | 121 |
| G342.48+0.18 | Y | 16515−4308 | 51 |
| G344.23−0.57 | Y | 17006−4215 | 94 |
| | 25/36 | avg./median | 84/50 |
| Table 3 | | | |
| G11.11−0.11 | Y | 18073−1923 | 104 |
| G16.58−0.08 | Y | 18182−1433 | 125 |
| G24.63+0.15 | Y | 18331−0717 | 281 |
| G29.84−0.47 | Y | 18446−0303 | 190 |
| G29.96−0.79 | Y | 18461−0304 | 35 |
| G34.28+0.18 | Y | 18507+0110 | 170 |
| G40.28−0.22 | Y | 19031+0621 | 73 |
| G45.80−0.36 | N | 19141+1110 | 10 |
| G49.07−0.33 | Y | 19205+1403 | 179 |
| G49.27−0.32 | N | 19207+1410 | 252 |
| G50.36−0.42 | Y | 19234+1510 | 144 |
| G53.92−0.07 | N | 19291+1826 | 20 |
| G54.11−0.08 | N | 19294+1836 | 89 |
| G54.45+1.01 | N | 19262+1925 | 9 |
| G58.79+0.63 | N | 19366+2301 | 105 |
| G62.70−0.51 | N | 19497+2549 | 14 |
| G304.89+0.64 | Y | 13050−6154 | 6 |
| G309.91+0.32 | Y | 13475−6129 | 69 |
| G309.97+0.59 | Y | 13475−6115 | 169 |
| G309.99+0.51(b) | Y | 13475−6115 | 142 |
| G311.51−0.45 | Y | 14023−6150A | 101 |
| G324.11+0.44 | Y | 15272−5533 | 2 |
| G326.36+0.88 | Y | 15375−5352 | 308 |
| G326.41+0.93 | Y | 15384−5348 | 160 |
| G326.57+0.20 | N | 15422−5418 | 112 |
| G326.61+0.80(a) | Y | 15395−5348 | 102 |
| G326.61+0.80(c) | Y | 15395−5348 | 95 |
| G326.65+0.75 | Y | 15402−5349 | 12 |
| G326.80+0.51 | Y | 15415−5356 | 217 |
| G326.92−0.31 | Y | 15462−5428 | 110 |
| G327.30−0.58 | Y | 15492−5426 | 101 |
| G327.72−0.38 | N | 15508−5403 | 84 |
| G327.86+0.19 | N | 15489−5333 | 121 |
| G327.89+0.15 | Y | 15489−5333 | 228 |
| G328.55+0.27 | Y | 15522−5301 | 12 |
| G329.07−0.31(a) | Y | 15573−5307 | 17 |
| G329.07−0.31(b) | Y | 15573−5307 | 1 |
| G329.16−0.29 | Y | 15579−5303 | 120 |
| G329.18−0.30 | Y | 15579−5303 | 30 |
| G331.08−0.47 | Y | 16076−5154 | 161 |
| G331.37−0.40 | Y | 16089−5137 | 154 |
| G331.62+0.53 | N | 16061−5048 | 21 |
| G331.71+0.58 | Y | 16062−5041 | 70 |
| G331.71+0.60 | Y | 16062−5041 | 3 |
| G332.28−0.07 | Y | 16119−5048 | 100 |
| G332.33−0.12 | Y | 16122−5047 | 61 |
| G332.36+0.60 | Y | 16093−5015 | 38 |
| G332.47−0.52 | Y | 16147−5100 | 47 |
| G332.58+0.15 | Y | 16122−5028 | 167 |
| G332.59+0.04(a) | Y | 16128−5033 | 185 |
| G332.59+0.04(b) | Y | 16128−5033 | 193 |
| G332.91−0.55 | Y | 16168−5044 | 156 |

**Table 6**
(Continued)

| Name (1) | IRDC? (2) | Nearest *IRAS* PS[a] (3) | Angular Separation (″) (4) |
|---|---|---|---|
| G333.08−0.56 | Y | 16172−5032 | 278 |
| G334.04+0.35 | N | 16178−4916 | 7 |
| G334.25+0.07 | Y | 16200−4919 | 48 |
| G335.43−0.24 | Y | 16264−4841 | 77 |
| G336.87+0.29 | Y | 16301−4718 | 138 |
| G336.96−0.98 | Y | 16358−4804 | 32 |
| G337.16−0.39 | Y | 16340−4732 | 22 |
| G338.32−0.41 | Y | 16389−4639 | 129 |
| G340.75−1.00 | Y | 16506−4512 | 161 |
| G340.77−0.12 | Y | 16465−4437 | 126 |
| G340.78−0.10 | N | 16465−4437 | 52 |
| G341.20−0.26 | Y | 16487−4423 | 110 |
| G341.23−0.27 | Y | 16487−4423 | 141 |
| G342.15+0.51 | N | 16489−4318 | 453 |
| G342.90−0.12 | N | 16541−4259 | 41 |
| G343.19−0.08(a) | Y | 16550−4245 | 10 |
| G343.40−0.40 | Y | 16566−4249 | 345 |
| G343.42−0.33 | Y | 16573−4240 | 342 |
| G343.50+0.03 | Y | 16558−4228 | 158 |
| G343.53−0.51(a) | Y | 16579−4245 | 45 |
| G343.78−0.24 | Y | 16576−4223 | 8 |
| G344.21−0.62 | N | 17006−4215 | 95 |
| G348.17+0.46 | N | 17089−3834 | 383 |
| | 58/75 | avg./median | 116/102 |
| Table 4 | | | |
| G12.2−0.03 | N | 18094−1823 | 22 |
| G12.42+0.50 | N | 18079−1756 | 12 |
| G12.68−0.18 | N | 18112−1801 | 206 |
| G17.96+0.08 | N | 18205−1316 | 12 |
| G19.61−0.14 | N | 18244−1155 | 13 |
| G20.24+0.07 | N | 18249−1116 | 10 |
| G21.24+0.19 | Y | 18263−1020 | 19 |
| G23.82+0.38 | N | 18305−0758 | 22 |
| G24.11−0.17 | Y | 18334−0757 | 216 |
| G24.11−0.18 | Y | 18334−0757 | 210 |
| G24.33+0.14 | Y | 18324−0737 | 5 |
| G28.85−0.23 | N | 18421−0348 | 78 |
| G29.89−0.77 | Y | 18460−0307 | 25 |
| G29.91−0.81 | N | 18460−0307 | 128 |
| G35.83−0.20 | Y | 18549+0226 | 83 |
| G39.39−0.14 | N | 19012+0536 | 4 |
| G40.60−0.72 | N | 19056+0624 | 8 |
| G43.04−0.45(a) | N | 19092+0841 | 24 |
| G43.04−0.45(b) | N | 19092+0841 | 25 |
| G45.47+0.13 | N | 19117+1107 | 21 |
| G45.50+0.12 | N | 19117+1107 | 91 |
| G49.91+0.37 | N | 19195+1508 | 5 |
| G54.11−0.04 | N | 19294+1836 | 89 |
| G54.11−0.05 | N | 19294+1836 | 73 |
| G57.61+0.02 | N | 19365+2142 | 18 |
| G58.78+0.64 | N | 19366+2301 | 23 |
| G58.78+0.65 | N | 19366+2301 | 21 |
| G305.77−0.25 | N | 13134−6242 | 91 |
| G305.80−0.24 | N | 13134−6242 | 17 |
| G309.38−0.13(b) | Y | 13438−6203 | 32 |
| G309.97+0.50 | Y | 13475−6115 | 184 |
| G309.99+0.51(c) | Y | 13475−6115 | 149 |
| G310.15+0.76 | N | 13484−6100 | 14 |
| G310.38−0.30(a) | Y | 13524−6159 | 9 |
| G310.38−0.30(b) | Y | 13524−6159 | 13 |
| G310.38−0.30(c) | Y | 13524−6159 | 24 |
| G310.38−0.30(d) | Y | 13524−6159 | 17 |

**Table 6**
(Continued)

| Name (1) | IRDC? (2) | Nearest *IRAS* PS[a] (3) | Angular Separation (″) (4) |
|---|---|---|---|
| G311.04+0.69 | Y | 13558−6051 | 57 |
| G313.71−0.19(a) | Y | 14188−6054 | 37 |
| G313.71−0.19(b) | Y | 14188−6054 | 33 |
| G313.76−0.86 | Y | 14212−6131 | 11 |
| G317.44−0.37 | Y | 14467−5939 | 242 |
| G320.24−0.29 | Y | 15061−5814 | 64 |
| G323.74−0.26 | N | 15278−5620 | 30 |
| G325.52+0.42 | N | 15353−5445 | 12 |
| G326.37+0.94 | Y | 15375−5352 | 233 |
| G326.64+0.76 | Y | 15402−5349 | 52 |
| G326.99−0.03 | Y | 15453−5416 | 151 |
| G327.57−0.85 | Y | 15519−5430 | 29 |
| G327.65+0.13 | N | 15481−5341 | 2 |
| G328.16+0.59 | N | 15488−5300 | 1 |
| G328.60+0.27 | Y | 15522−5301 | 163 |
| G328.81+0.63 | Y | 15520−5234 | 4 |
| G330.95−0.18 | Y | 16060−5146 | 35 |
| G331.12−0.46 | Y | 16082−5150 | 158 |
| G331.34−0.35 | N | 16085−5138 | 41 |
| G331.51−0.34 | Y | 16093−5128 | 168 |
| G332.28−0.55 | Y | 16141−5107 | 159 |
| G332.29−0.09 | N | 16119−5048 | 10 |
| G332.29−0.55 | Y | 16141−5107 | 129 |
| G332.35−0.44 | Y | 16137−5100 | 10 |
| G333.13−0.56 | N | 16178−5029 | 237 |
| G333.32+0.10 | Y | 16157−4957 | 2 |
| G335.59−0.30 | Y | 16272−4837 | 63 |
| G336.02−0.83 | N | 16313−4840 | 33 |
| G336.03−0.82 | N | 16313−4840 | 27 |
| G337.40−0.40 | Y | 16351−4722 | 8 |
| G338.42−0.41 | Y | 16390−4637 | 95 |
| G338.92+0.55(a) | N | 16368−4538 | 171 |
| G338.92+0.55(b) | N | 16368−4538 | 151 |
| G339.58−0.13 | Y | 16424−4531 | 139 |
| G340.05−0.25 | Y | 16445−4516 | 34 |
| G340.06−0.23 | Y | 16445−4516 | 43 |
| G340.07−0.24 | Y | 16445−4516 | 51 |
| G340.10−0.18 | N | 16442−4511 | 169 |
| G340.76−0.12 | Y | 16465−4437 | 130 |
| G341.22−0.26(b) | Y | 16487−4423 | 102 |
| G342.04+0.43 | N | 16489−4318 | 77 |
| G343.19−0.08(b) | Y | 16550−4245 | 22 |
| G343.42−0.37 | Y | 16573−4240 | 331 |
| G343.53−0.51(b) | Y | 16579−4245 | 51 |
| G344.22−0.57 | Y | 17006−4215 | 89 |
| G345.00−0.22(a) | Y | 17016−4124 | 16 |
| G345.00−0.22(b) | Y | 17016−4124 | 15 |
| G345.13−0.17 | N | 17020−4117 | 129 |
| G346.04+0.05 | N | 17038−4026 | 60 |
| G346.28+0.59 | N | 17023−3954 | 16 |
| G348.18+0.48 | N | 17089−3820 | 404 |
| G348.72−1.04 | Y | 17167−3854 | 40 |
| G348.73−1.04 | Y | 17167−3854 | 39 |
| | 49/90 | avg./median | 73/36 |
| Outflow-only (Table 5) | | | |
| G12.91−0.26 | N | 18117−1753 | 8 |
| G34.26+0.15 | N | 18507+0110 | 56 |
| G37.55+0.20 | N | 18566+0408 | 39 |
| G345.51+0.35 | N | 17008−4040 | 55 |
| | 0/4 | avg./median | 40/47 |

**Note.** [a] B1950 coordinates.

**Table 7**
6.7GHz $CH_3OH$ Maser Associations of EGOs

| Name (1) | Maser Survey[a] (2) | Walsh *IRAS* Target[b] (3) | Maser?[a] (4) | Offset (″)[c] (5) | Distance (kpc)[d] (6) |
|---|---|---|---|---|---|
| Table 1 | | | | | |
| G11.92−0.61 | W | 18110−1854 | N | | |
| G14.33−0.64 | W | 18159−1648 | N | | |
| G28.83−0.25 | W | 18421−0348 | Y | 3 | |
| G298.26+0.74 | W | 12091−6129 | Y | <1 | |
| G312.11+0.26 | W | 14050−6056 | Y | 1 | |
| G326.27−0.49 | E | | N | | |
| G326.78−0.24 | E | | N | | |
| G326.79+0.38 | E | | N | | |
| G326.86−0.67[e] | E | | Y | 5 | 3.7 |
| G326.97−0.03 | E | | N | | |
| G327.12+0.51 | W, E | 15437−5343 | Y (W, E) | 1 | 5.5 |
| G327.39+0.20 | E | | Y | <1 | 5.3 |
| G327.40+0.44 | E | | Y | 5 | 5.2 |
| G328.14−0.43 | E | | N | | |
| G329.18−0.31 | E | | Y | 3 | 3.6 |
| G329.47+0.52 | W, E | 15557−5215 | Y (W) | <1 | 4.5 |
| G329.61+0.11 | E | | Y | <1 | 3.9 |
| G332.35−0.12 | C, E | | N | | |
| G332.56−0.15 | C, W, E | 16132−5039 | Y (C, W, E) | 2 | 3.5 |
| G332.94−0.69[e] | E | | Y | 1 | 3.6 |
| G333.18−0.09 | C, E | 16159−5012 | Y (C, E, W could not locate) | 1 | 5 |
| G335.59−0.29 | C, W, E | 16272−4837 | Y (C, W) | 2, 4, 17 | |
| G339.95−0.54 | W | 16455−4531 | Y | 1 | |
| G343.12−0.06 | W | 16547−4247 | N | | |
| G344.58−0.02 | W | 16594−4137 | Y | <1 | |
| Table 2 | | | | | |
| G10.29−0.13 | W | 18060−2005 | Y | 2 | |
| G10.34−0.14 | W | 18060−2005 | Y | <1 | |
| G16.59−0.05 | W | 18182−1433 | Y | <1 | |
| G19.36−0.03 | W | 18236−1205 | Y | 4 | |
| G19.61−0.12 | W | 18244−1155 | Y | 5 | |
| G28.28−0.36 | W | 18416−0420 | Y | 1 | |
| G320.23−0.28 | W | 15061−5814 | Y | 6 | |
| G326.32−0.39 | E | | N | | |
| G326.47+0.70[e] | E | | Y? | 11 | 2.6 |
| G326.48+0.70[e] | E | | Y? | 8 | 2.6 |
| G328.25−0.53 | E | | Y | 1 | 2.6 |
| G329.03−0.20 | E | | Y | 7, 19 | 2.6, 2.9 |
| G329.41−0.46 | W, E | 15596−5301 | Y (E) | 3 | 4.2 |
| G329.47+0.50 | W, E | 15557−5215 | Y | 3 | 4.5 |
| G330.88−0.37 | W, E | 16065−5158 | N | | |
| G331.13−0.24 | W, E | 16071−5142 | Y (W, E) | 3 | 5.2 |
| G332.60−0.17 | C, E | | Y (C, E) | <1 | 3.5 |
| G332.73−0.62 | W | 16158−5055 | Y | 1 | |
| G333.47−0.16 | C, W, E | 16175−5002 | Y (C, W, E) | 1 | 3 |
| G335.06−0.43 | E | | Y | <1 | 3.4 |
| G335.79+0.18 | C | | Y | 5 | |
| G337.91−0.48 | W | 16374−4701 | N | | |
| G344.23−0.57 | W | 17006−4215 | Y | 7, 8 | |
| Table 3 | | | | | |
| G16.58−0.08 | W | 18182−1433 | N | | |
| G326.57+0.20 | E | | N | | |
| G326.80+0.51 | E | | N | | |
| G326.92−0.31 | E | | N | | |
| G327.72−0.38 | E | | N | | |
| G327.86+0.19 | E | | N | | |
| G327.89+0.15 | E | | N | | |
| G328.55+0.27 | E | | N | | |
| G329.07−0.31(a) | E | | N | | |
| G329.07−0.31(b) | E | | Y | <1 | 3 |
| G329.16−0.29 | E | | N | | |
| G329.18−0.30 | E | | N | | |
| G331.08−0.47 | E | | N | | |
| G331.37−0.40 | W, E | 16085−5138 | N | | |

**Table 7**
(Continued)

| Name (1) | Maser Survey[a] (2) | Walsh *IRAS* Target[b] (3) | Maser?[a] (4) | Offset (″)[c] (5) | Distance (kpc)[d] (6) |
|---|---|---|---|---|---|
| G331.62+0.53 | E | | N | | |
| G332.28−0.07 | C, E | | N | | |
| G332.33−0.12 | C, E | | N | | |
| G332.47−0.52 | E | | N | | |
| G332.58+0.15 | C, E | | N | | |
| G332.59+0.04(a) | C, E | | N | | |
| G332.59+0.04(b) | C, E | | N | | |
| G334.04+0.35 | E | | N | | |
| G334.25+0.07 | C, E | | N | | |
| G340.75−1.00 | W | 16506−4512 | N | | |
| G343.19−0.08(a) | W | 16547−4247 | N | | |
| G344.21−0.62 | W | 17006−4215 | N | | |
| Table 4 | | | | | |
| G19.61−0.14 | W | 18244−1155 | N | | |
| G28.85−0.23 | W | 18421−0348 | Y | 2 | |
| G305.77−0.25 | W | 13134−6242 | N | | |
| G305.80−0.24 | W | 13134−6242 | N | | |
| G309.97+0.50 | W | 13471−6120 | N | | |
| G313.76−0.86 | W | 14212−6131 | Y | 3, 25 | |
| G320.24−0.29 | W | 15061−5814 | N | | |
| G323.74−0.26 | W | 15278−5620 | Y | 0.6, 0.8, 3 | |
| G325.52+0.42 | E | | N | | |
| G326.99−0.03 | E | | N | | |
| G327.65+0.13 | E | | N | | |
| G328.60+0.27 | E | | N | | |
| G328.81+0.63 | W, E | 15520−5234 | Y (W, E) | <1 | 3 |
| G330.95−0.18 | C, W, E | 16060−5146 | Y (W, E) | 3 | 5.3 |
| G331.12−0.46 | E | | N | | |
| G331.34−0.35 | W, E | 16085−5138 | Y (W, E) | 1 | 4.3 |
| G331.51−0.34 | E | | N | | |
| G332.29−0.09 | C, E | | Y (E) | 3 | 3.2 |
| G332.35−0.44 | E | | Y | 2 | 3.6 |
| G333.13−0.56[e] | E | | Y | 10 | 3.8 |
| G333.32+0.10 | C, E | | Y (C, E) | 2 | 3.1 |
| G335.59−0.30 | W | 16272−4837 | N | | |
| G336.02−0.83 | W | 16313−4840 | Y | 5 | |
| G336.03−0.82 | W | 16313−4840 | N | | |
| G337.40−0.40 | W | 16351−4722 | Y | 3, 4 | |
| G339.58−0.13 | C | 16424−4531 and 16421−4532 | Y | 8 | |
| G340.05−0.25 | W | 16445−4516 | Y | 12 | |
| G340.06−0.23 | W | 16445−4516 | N | | |
| G340.07−0.24 | W | 16445−4516 | N | | |
| G343.19−0.08(b) | W | 16547−4247 | N | | |
| G344.22−0.57 | W | 17006−4215 | N | | |
| G345.00−0.22(a) | W | 17016−4124 | Y | 4, 5 | |
| G345.00−0.22(b) | W | 17016−4124 | N | | |
| G348.72−1.04 | W | 17167−3854 | N | | |
| G348.73−1.04 | W | 17167−3854 | Y | <1 | |
| Outflow-only (Table 5) | | | | | |
| G12.91−0.26 | W | 18117−1753 | Y | <1 | |
| G345.51+0.35 | W | 17008−4040 | Y | 32 | |

**Notes.**

[a] C, Caswell (1996); W, Walsh et al. (1998); E, Ellingsen (2006).

[b] B1950 coordinates.

[c] Nominal separation from EGO positions listed in Tables 1–5, rounded to the nearest arcsecond. Separations less than 1″ are denoted as "<1." Where multiple offsets are listed, multiple spatially distinct maser spots are reported.

[d] Distances are the near kinematic distances reported in Ellingsen (2006). The association of EGOs with IRDCs supports the adoption of the near kinematic distance.

[e] Source outside the nominal area of Ellingsen et al. (1996) and Ellingsen (2006) of $325^\circ < l < 335^\circ$, $b = \pm 0.^\circ 53$ and not included in the calculation of the fraction of EGOs within the survey coverage that have associated 6.7 GHz $CH_3OH$ masers.

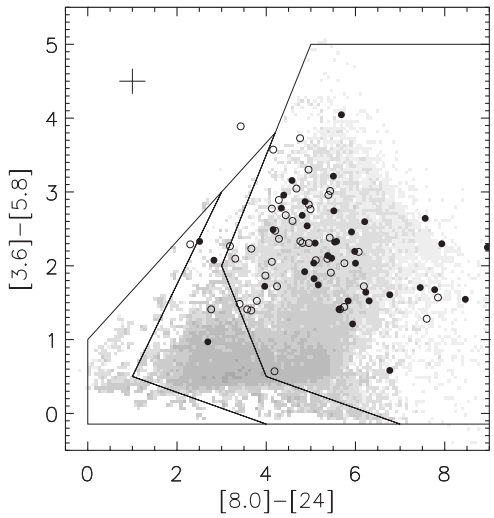


**Figure 13.** The Color–color plot of EGOs in Tables 1 (filled circles) and Table 3 (open circles). The error bar in the top left was derived from the average standard deviation of the measurements (Tables 1 and 3), converted to magnitudes and propagated to colors. The EGO points are overlaid on a grid of YSO models in gray scale (Robitaille et al. 2006). The black lines indicate regions occupied predominantly by models of various evolutionary stages: (right) the youngest sources surrounded by infalling envelopes (Stage I); (middle) more evolved sources surrounded by disks (Stage II), and (left) sources with low-mass disks (Stage III). Note that most EGOS fall in the region occupied by the youngest protostar models. EGOs with fluxes flagged as saturated or as upper limits in Tables 1 and 3 were excluded from the plot.

provided by NASA/JPL through contract 1289524. C.J.C. is supported by a National Science Foundation Graduate Research Fellowship.

## REFERENCES

Araya, E., et al. 2007, ApJ, 669, 1050
Benjamin, R. A., et al. 2003, PASP, 115, 953
Caswell, J. L. 1996, MNRAS, 279, 79
Cragg, D. M., Sobolev, A. M., & Godfrey, P. D. 2005, MNRAS, 360, 533
Cyganowski, C. J., Brogan, C. L., & Hunter, T. R. 2007, AJ, 134, 346
Dame, T. M., Hartmann, D., & Thaddeus, P. 2001, ApJ, 547, 792
Davis, C. J., Kumar, M. S. N., Sandell, G., Froebrich, D., Smith, M. D., & Currie, M. J. 2007, MNRAS, 374, 29
De Buizer, J. M. 2003, MNRAS, 341, 277
Ellingsen, S. P. 2006, ApJ, 638, 241
Ellingsen, S. P. 2007, MNRAS, 377, 571
Ellingsen, S. P., von Bibra, M. L., McCulloch, P. M., Norris, R. P., Deshpande, A. A., & Phillips, C. J. 1996, MNRAS, 280, 378
Fazio, et al. 2004, ApJS, 154, 10
Gutermuth, R. A., et al. 2008, ApJ, 674, 336
Hoare, M. G., Lumsden, S. L., Oudmaijer, R. D., Busfield, A. L., King, T. L., & Moore, T. L. J. 2004, ASP Conf. Ser. 317, ed. D. Clemens, R. Shah, & T. Brainerd (San Francisco, CA: ASP), 156
Hoare, M. G., et al. 2005, IAU Symp. 227, ed. R. Cesaroni et al. (Dordrecht: Kluwer), 370
Hunter, T. R., Brogan, C. L., Megeath, S. T., Menten, K. M., Beuther, H., & Thorwirth, S. 2006, ApJ, 649, 888
Indebetouw, R., et al. 2005, ApJ, 619, 931
Jackson, J. M., et al. 2006, ApJS, 163, 145
Minier, V., Ellingsen, S. P., Norris, R. P., & Booth, R. S. 2003, A&A, 403, 1095
Molinari, S., Brand, J., Cesaroni, R., & Palla, F. 1996, A&A, 308, 573
Neufeld, D. A., & Yuan, Y. 2008, ApJ, 678, 974
Noreiga-Crespo, A., et al. 2004, ApJS, 154, 352
Rathborne, J. M., Simon, R., & Jackson, J. M. 2007, ApJ, 662, 1082
Rathborne, J. M., Jackson, J. M., & Simon, R. 2006, ApJ, 641, 389
Rathborne, J. M., Jackson, J. M., Chambers, E. T., Simon, R., Shipman, R., & Frieswijk, W. 2005, ApJ, 630, L181
Reach, W. T., et al. 2006, AJ, 131, 1479
Rieke, G. H., et al. 2004, ApJS, 154, 25
Robitaille, T. P., Whitney, B. A., Indebetouw, R., Wood, K., & Denzmore, P. 2006, ApJS, 167, 256
Shepherd, D. S., et al. 2007, ApJ, 669, 464
Simon, R., Jackson, J. M., Rathborne, J. M., & Chambers, E. T. 2006, ApJ, 639, 227
Simon, R., Rathborne, J. M., Shah, R. Y., Jackson, J. M., & Chambers, E. T. 2006, ApJ, 653, 1325
Smith, H. A., Hora, J. L., Marengo, M., & Pipher, J. L. 2006, ApJ, 645, 1264
Smith, M. D., & Rosen, A. 2005, MNRAS, 357, 1370
Sridharan, T. K., Beuther, H., Schilke, P., Menten, K. M., & Wyrowski, F. 2002, ApJ, 566, 931
Szymczak, M., Pillai, T., & Menten, K. M. 2005, A&A, 434, 613
Urquhart, J. S., Hoare, M. G., Lumsden, S. L., Oudmaijer, R. D., & Moore, T. J. T. 2008, ASP Conf. Ser. 387, ed. H. Beuther, H. Linz, & T. Henning (San Francisco, CA: ASP), 381
Velusamy, T., Langer, W. D., & Marsh, K. A. 2007, ApJ, 668, L159
Walsh, A. J., Burton, M. G., Hyland, A. R., & Robinson, G. 1998, MNRAS, 301, 640
Yusef-Zadeh, F., et al. 2007, in IAU Symp. 242, Astrophysical Masers & Their Environments, ed. J. M. Chapman & W. A. Baan (Dordrecht: Kluwer), 366
Zinnecker, H., & Yorke, H. W. 2007, ARA&A, 45, 481